ISSN 1849-0751 (On-line)
ISSN 0013-7448 (Print)
UDK 621.31

Journal of Energy

VOLUME 67 | 2018 Special Issue

ENERGIJA 67

Journal of Energy

Scientific Professional Journal Of Energy, Electricity, Power Systems

Online ISSN 1849–0751, Print ISSN 0013–7448, VOL 66

Published by

HEP d.d., Ulica grada Vukovara 37, HR–10000 Zagreb

HRO CIGRÉ, Berislavićeva 6, HR–10000 Zagreb

EDITORIAL

Journal of Energy special issue: Papers from First International Colloquium on Smart Grid Metrology (Smagrimet 2018)

Welcome to this special issue of the Journal of Energy, dedicated to the publication of extended versions of some of the selected papers presented at the First International Colloquium on Smart Grid Metrology (Smagrimet 2018), held in Podstrana (Split), Croatia, from 24th to 27th April, 2018.

This Colloquium was organized by University of Zagreb, Faculty of electrical engineering and computing (FER) in cooperation with University of Split, Faculty of Electrical Engineering, Mechanical Engineering and Naval Architecture (FESB). It was also supported by Croatian branch of the International council for large electric power systems (HRO-CIGRE) with technical co-sponsorship from IEEE Instrumentation and Measurement Croatia Chapter.

The principal goal of this new event has been to address effective development and deployment of smart grids as well as in broad range of accompanying applications such as wireless and optical sensors, smart cities and vehicles, medicine, signal processing, machine learning, energy management and beyond. In that way Colloquium provided an environment for exchanging university and industrial experience, knowledge and ideas in the form of oral and poster sessions, invited speaker presentations and special sessions organized by the industry.

From 44 papers presented at the Colloquium, 4 papers were accepted for publication in this number of Journal of Energy after having undergone the additional peer-review process. We would like to thank the authors for their contributions and the reviewers who dedicated their valuable time in selecting and reviewing these papers, both during the Conference and during the preparation of this special issue of Journal of Energy. It was very challenging to collect a balanced overview of the entire Conference. We decided to select 4 papers for this issue and additional ones for the next issue.

We believe that the papers which were selected for this issue represent some of the best research related to development of new measurement procedures and calibration standards in the area of power and energy metrology.

The high quality of the four papers contained in this special issue is the result of the cooperation of a number of people: the authors, who submitted their very best work to the Journal; the referees, who helped in the selection of the published papers; and finally, the many people at HRO-CIGRE who assisted us in the production phase. We sincerely thank them all for their help to make this special issue possible.

July 2018

Guest Editor
Marko Jurčević
University of Zagreb, Croatia

Journal of Energy

VOLUME 67 | 2018

journal homepage: http://journalofenergy.com/

A Circular Loop Time Constant Standard

Martin Dadić
University of Zagreb
Faculty of Electrical Engineering and Computing / FER
Zagreb, Croatia, martin.dadic@fer.hr

Monika Sandelić
Aalborg University
Department of Energy Technology,
Aalborg, Denmark, msande16@student.aau.dk

Hrvoje Hegeduš
University of Zagreb
Faculty of Electrical Engineering and Computing / FER
Zagreb, Croatia, hrvoje.hegedus@fer.hr

Goran Petrović
University of Split
Faculty of Electrical Engineering, Mechanical Engineering and Naval Architecture
Split, Croatia, goran.petrovic@fesb.hr

Summary

A time constant standard, developed for the phase angle measurement of precision current shunts is developed and described, and its time constant has been determined. Based on a single circular loop placed in an air thermostat, its construction is very simple and it gives accurate results in the frequency band of interest, e.g. for frequencies between 50 Hz and 100 kHz. The influence of the shielding is calculated using numerical Finite Element Analysis (FEA). The thermostatic stability is analyzed, and the time-constant of the thermostat is determined using temperature measurement and Butterworth filtering. The power coefficient of the standard is determined, and limits of errors are discussed.

Key words: time constant standard, circular loop, phase angle measurment, thermostat, Finite Element Method (FEM)

Introduction

An increased interest in correct measurement of current over a wide frequency range is triggered by a widespread application of equipment like power converters, power electronics and nonlinear loads, which produce higher harmonics. Therefore, the phase angle reference is important for the determination of the phase angle errors of precision AC/DC shunts. Additionally, it is also needed in other applications like capacitor loss factor calibration. Classical designs of calculable resistors include Haddad, bifilar and folded loops [1,2]. In [3] a simple resistance standard with calculable time constant is described. In [4] a coaxial time constant standard for the determination of phase angle errors of current shunt is presented.

The main goal of this paper is to present a time constant standard for the determination of phase angle errors of current shunts, using a recently developed phase comparator based on a PXI NI 4461 system and LabView environment. While it is generally possible to match the parasitic inductance and capacitance to resistance of the standard in such a way that the time constant is as close as possible to zero [2],[3], it is decided, due to the computational flexibility of the LabView to digitally compensate the phase lag of the standard instead. This allows simpler design and easier manufacturing of the standard. The targeted frequency bandwidth of the standard is 50 Hz - 100 kHz.

Design of Circular Loop Standard

The standard is based on a single circular loop. If the diameter of the wire is chosen to be sufficiently small comparing to the skin depth, its inductance and resistance will be constant over the desired frequency bandwidth, and it is easily precisely calculated. In comparison to the bifilar and folded loops, the mutual inductance does not exist, as well as the proximity effect and the parasitic capacitance between loops. The main difference between the actual inductance and the inductance of the ideal circular loop is a small gap in the loop needed for the connection of the external cables. To cope with this effect, it is decided to measure the inductance using a precision LCR bridge instead of using the calculated inductance values. The loop is mounted in a massive passive aluminum thermostat, which serves in the same time as the electrostatic shield of the system and averages the ambient temperature changes. The equivalent circuit of the time constant standard is depicted in Fig. 1.

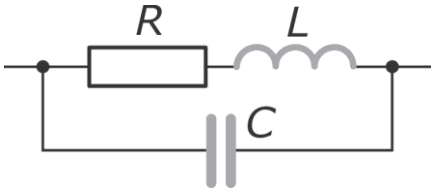

Figure 1. Equivalent circuit of the resistor

The resistance is, as well as the inductance constant over the frequency bandwidth of interest if the wire diameter is sufficiently small in comparison with the skin depth. The inductance will be, for the mounted loop in the electrically conductive thermostat, generally frequency dependent to the some level, which is investigated using the Finite Element Analysis (FEA). The capacitance *C* is defined by the capacitance of the cables, which was measured using a LCR bridge.

The time constant τ can be expressed approximately for most values of *R* and *C* as [3-5]

$$\tau = \frac{L}{R} - RC \tag{1}$$

with the phase angle of the standard

$$\varphi = 2\pi f \times \tau \tag{2}$$

The circular loop is wound using a manganin wire with the diameter 0.07 mm on a circular plastic former (Fig. 2). For the easier assembling, a circular gutter was machined in the former. The radius of the manganin loop (taking into account the gutter depth and the radius of the former) was fi-

nally 25.035 mm. The loop is connected with two coaxial cables Amphenol RG 223U, for the 4-wire connection in the external bridge circuit. The current cable is equipped with a N-type connector that matches our serial T-piece, while the sense (potential) cable is equipped with a BNC connector. The sleeve of the sense cable is connected to the shield (thermostat), thus forming the electrostatic shield and shunting the capacitance between the loop and the shield.

Figure 2. Former with the circular loop mounted on the top plate of the thermostat

Analytical Calculation of the Inductance

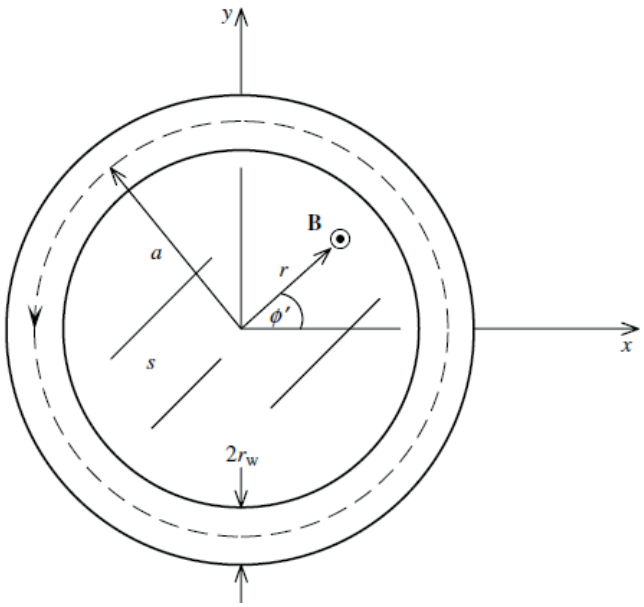

Figure 3. Model of the circular loop wire

The inductance of the circular loop (Fig. 3) can be calculated analytically approximately as [6]

$$L = \mu a\left(\ln\left(\frac{8a}{r_w}\right) - \frac{3}{2}\right) \tag{3}$$

Here, denotes radius of the loop, wire radius is andis permeability of the air. It is, further on, assumed that current is uniformly distributed over the entire cross section of the wire.

It should be pointed out that the expression (3) has certain inaccuracy based on the assumptions and approximations taken into account during deriving of the expression. The inaccuracy should be taken into account when using theoretically obtained values as reference points for further comparison with simulation and experimental results.

In Table I, dimensions of circular loop resistor and the obtained results of parasitic inductance are given.

Table I. Loop dimensions and analytically calculated inductance

a [mm]	r_w [mm]	L [μH]
25.035	0.035	0.225

Measurement of the Inductance

Figure 4. Inductance measurement

To determine the inductance L of the standard, the loop was initially wound using a copper wire with the same diameter, in the same manner as in [4]. In this way, the resistance is much smaller than the reactance of the loop, and at higher frequencies the inductance can be determined more precisely. The inductance was measured using a HP 4284A precision LCR meter using a custom-made test fixture (Fig. 4), open-short calibration and following settings: Integr: long, avg. 4, level 1 V and bias 0 V. In Table II, the measurement results are presented.

Table II. Measured inductance

f(kHz)	1	2	5	10	20
L(μH)	0.2240	0.2250	0.2240	0.2230	0.2240
R (Ω)	0.6164	0.6155	0.6156	0.6152	0.6152

f(kHz)	50	100	150	200	250
L(μH)	0.2240	0.2215	0.2207	0.2202	0.2198
R (Ω)	0.6158	0.6171	0.6171	0.6176	0.6173

f(kHz)	300	333.33	400	480	500
L(μH)	0.2195	0.2190	0.2191	0.2188	0.2187
R (Ω)	0.6185	0.6192	0.6196	0.6208	0.6210

From the Table II it may be concluded that the inductance and resistance does not change in the frequency band bellow 500 kHz. Above 500 kHz the results were inconsistent, which may be attributed to the test fixture, the parasitic capacitance or the calibration of the bridge.

Using all this information, the chosen inductance of the standard is the inductance measured in the middle of the measured frequency band, e.g. at 250 kHz, which is 0.2198 μH. The accuracy of the bridge is % of reading.

FEM Analysis

Conducting and magnetic shields are commonly used in prevention of undesired coupling among different coils and in reduction of the electromagnetic noise [7,8].

When a conducting shield is placed in the vicinity of the conductor, it changes magnetic field distribution produced by the current by open- circuiting the magnetic path. As a result, the eddy currents are induced in the shield and they couple with source current in a reverse manner. Therefore, the resultant magnetic field, in the vicinity of the source, is reduced. Consequently, the inductance of the circular loop wire inside the shield is reduced. Due to the fact that the effect of these phenomena is changing the inductance, its influence should be examined as to conclude if it can be neglected [9]. It was performed using the Finite Element Method (FEM) analysis.

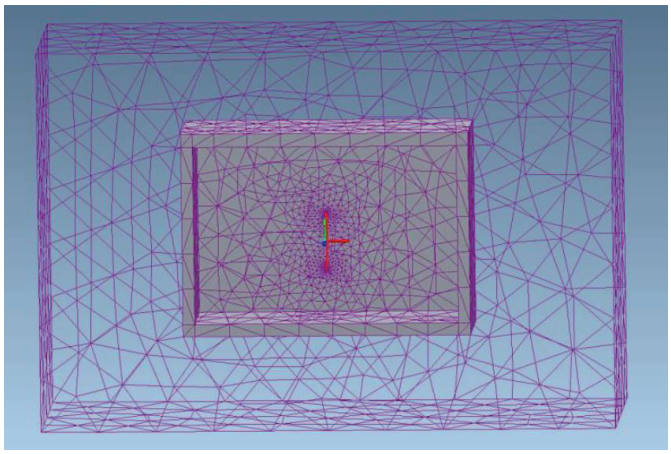

Figure 5. Mesh of finite elements

Simulations for the circular loop resistor were run in MagNet Infolytica software. The resistor is modeled according to the dimensions provided in Table I. Static and time harmonic simulations were performed. During static simulations, the maximum element size parameter has been adjusted in order to determine influence of the FEM grid construction on the obtained results. It was found that for the values of maximum element size equal to or smaller then 0.1 mm, the simulation results do not deviate much from theoretically obtained value. Therefore, it is decided that the maximum element size is set to 0.15 mm for further time harmonic simulations. In addition, it should be pointed out that duration of the simulation process is an important parameter in determination of the optimal maximum element size value. As for better and more accurate results, the grid should be constructed of greater number of small elements, which consequently, require longer processing time.

For the maximum element size equal to 0.15 mm, the calculated inductance using FEM was 0.24913 μH.

The simulation results describing the influence of the electrostatic shield on copper wire inductance is shown in Fig. 3. As it may be observed, inductance value is higher for the case without electrostatic shield. The simulated results correspond to expected values based on the theory.

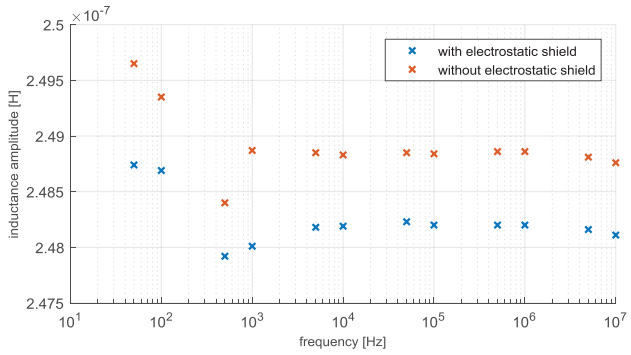

Figure 6. Change of inductance with the frequency for copper wire

The inductance values calculated using FEM follow the same trend with the frequency, with expected lower values for the shielded loop, due to the induced eddy currents in the shield (thermostat). The frequency dependence of the curve for the shielded case can be attributed to the skin effect, which influences the induced currents in the shield, and the errors in the simulations, which are inevitable. The biggest difference between shielded and un-shielded case in the calculated inductance (for the calculated set of frequencies) is at 50 Hz, and it is 0.3652 %. It should be added to the accuracy of the measurement of the inductance using the LCR bridge, since the measurements were performed without the shield. Fig. 6 also suggests the change of the inductance with the frequency (due to the errors in the simulations and the skin effect). The biggest difference for the shielded case relatively to the inductance calculated at 50 Hz (as the reference value) is at 500 Hz, and it equals 0.3284 %. In the conservative approach, it is also added to the overall accuracy of the measured inductance.

The calculated change of the resistance is 0.02 ppm at 100 kHz, using the same FEM model and the manganin wire (instead of copper).

Thermostat

Thermostatic stability is another characteristic that should be taken into consideration as it influences on resistance of the circular loop wire. The main reason why these effects are investigated experimentally is because they might have an influence on the resistor and its values when subjected to different working environments.

The measurement set-up was consisted of 8 NTC resistors (10 kΩ, Thermometrics MC65F103A) as the temperature sensors, connected to the digital multimeter DM3064. Two NTC resistors were placed out of the thermostat, 4 resistors were tight connected to the thick aluminum plates which form the air thermostat (within the thermostat). The last two resistors were placed in the air within the thermostat. The multimeter was connected to a PC computer, and the analysis and data acquisition process was performed using a LabView program developed for this purpose.

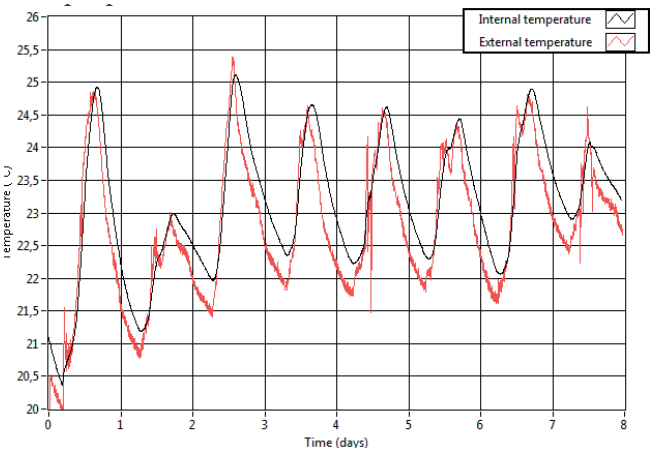

Figure 7. External and internal temperature of the thermostat during 8 days

Fig. 7 shows the changes of the internal temperature of the thermostat, compared to the ambient temperature. It is seen that the thermostat, due to its massive construction, efficiently cope with the transient, short-time variations in the ambient temperature, and that it introduces an expected delay in the global trend in the change of the temperature.

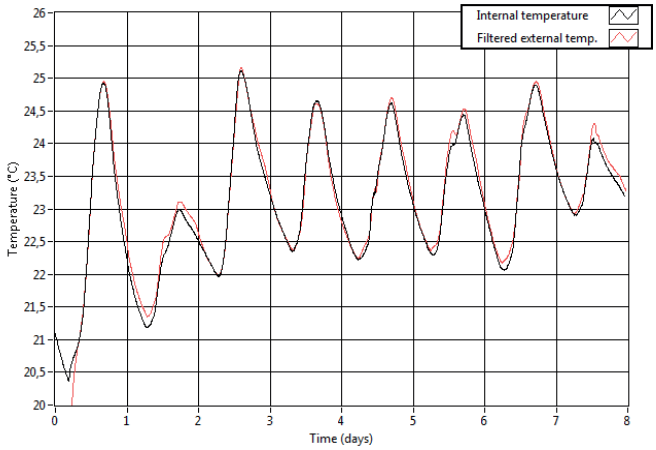

Figure 8. Filtered external vs. internal temperature of the thermostat

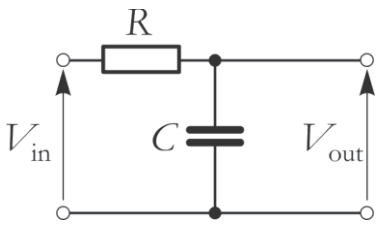

Figure 9. RC integrator circuit

The time-constant of the thermostat was estimated using the lumped heat-capacity approach [10]. The thermostat is as the thermal system consisted of the thermal capacitance and the thermal resistance. It exhibits filtering characteristics like an RC integrator circuit, depicted in Fig. 9. The frequency response (magnitude) of the RC integrator from Fig. 9 is

$$H_{RC}(\omega)=\frac{V_{out}}{V_{in}}=\frac{1/\omega C}{\sqrt{R^2+(1/\omega C)^2}}=\frac{1}{\sqrt{1+(\omega RC)^2}}=\frac{1}{\sqrt{1+(\omega/\omega_0)}} \quad (4)$$

Where C is the equivalent electric capacitance, R is equivalent electric resistance, ω denotes radian frequency and

$$\omega_0=\frac{1}{RC} \quad (5)$$

is – 3dB cutoff radian frequency of the integrator. It is forming a low-pass filter in the equivalent electrical network. Let's define the transfer function (magnitude) of a Butterworth filter of order n with the same cutoff radian frequency [11]:

$$H(\omega)=\frac{1}{\sqrt{1+\left(\frac{\omega}{\omega_0}\right)^{2n}}} \quad (6)$$

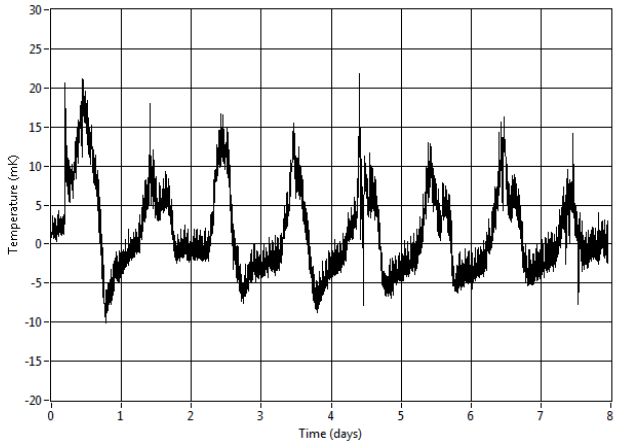

Figure 10. Difference between the temperature of the thermostat walls and the internal air temperature

For n=1 the transfer functions of the RC integrator and the Butterworth filter are the same. Therefore, to determine the cutoff frequency of the thermal system consisting the thermostat, the external temperature was filtered using a low-pass, first-order Butterworth filter. The filter was configured in LabView as the Infinite-Impulse-Response (IIR) digital filter. Its cutoff frequency was set in a manner that the low-pass filtered external temperature signal match in time the internal temperature (Fig. 8). The cutoff frequency was 28 μHz, which gives estimated time-constant of the system equal to 9.92 hours. The difference between the temperature of the thermostat walls and the internal air temperature is within 35 mK, and it is depicted in Fig. 10.

Measurement of Resistance and Capacitance

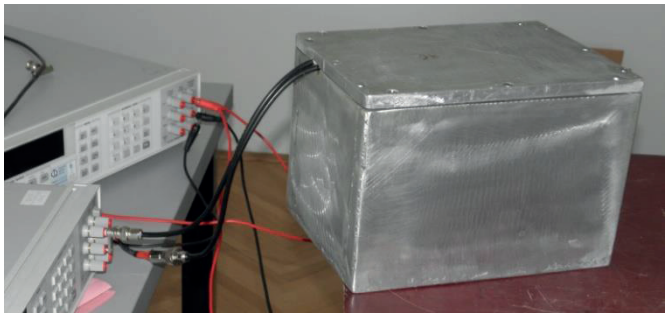

Figure 11. Assembled time constant standard during resistance measurement

The resistance was measured using an Agilent 3458A multimeter, with a 4-wire connection (Fig. 11). The measured DC resistance was R=20.16263 Ω, with the 2-year accuracy 20 ppm of reading + 10 ppm of range. For the 100 Ω range, the total accuracy is 1.4 mΩ, or 70 ppm of reading. The capacitance was measured using a Rohde&Schwarz (Hameg) HM8118 LCR bridge in 4-wire connection, using the Kelvin clamps. For the capacitance measurement, the cables were soldered in parallel (on the loop side) and the connectors were assembled, but the loop was not connected to the cables. Prior the measurement, the open-short calibration of the bridge was performed. The setting of the bridge was as follows: f=1 kHz, lev=1 V. The measured capacitance was C=96.091 pF. The accuracy of the measured capacitance is based on the equivalent impedance, which is 1.66 MΩ, and it equals 0.2104 %.

Power Coefficient

The power coefficient (PC) of the time constant standard influences its resistance, when it is used over wide range of currents. The power coefficient was characterized using a shunt of insignificant power coefficient (Method 4, [12]). At the Faculty of electrical engineering and computing, University of Zagreb, a set of cage type AC shunts has been produced [13, 14]. The PCs of shunts from this set, which have the rated currents less than 300 mA are insignificant. Therefore, the shunt with the rated current 100 mA was chosen as the reference standard (RSTD) for PC measurement. The circular loop resistance standard and RSTD were placed in series using a custom serial T-piece, while the current was supplied by a Rigol DP1116A DC single channel programmable power supply via a series resistor (1 kΩ for 10 mA current, and 100 Ω for 50 mA current). The current was monitored using a 61/2 digit digital multimeter (DMM) Rigol DM 3061, and the voltages across STD and circular loop resistance standard were measured using two 81/2 digit digital multimeter Agilent 3458A. The resistance ratio was measured for the currents equal to 10 mA and 50 mA, where the latter was chosen as the maximum current which still ensures that the voltage drop at the standard resistor fall within the 1 V range of DMM Agilent 3458A. The ratio of the voltages was measured after the time period that ensured that the loop resistor reached the constant resistance at each applied current. The determined PC is –3926 μΩ/Ω/W. The large PC is caused by the temperature coefficient of the manganin wire, together with a very small diameter of the wire. If the loop standard resistor is used with larger currents (50 mA or 70 mA), the correction of the resistance due to the power coefficient has to be included in the time-constant. If the applied current is kept at 10 mA, the change of the resistance due to the power coefficient (in the conservative approach, taking the PC as the constant) is –8 ppm, which can be included in the uncertainty, with a very small impact on the overall uncertainty. The resistance of the loop resistor, which was measured with DMM Agilent 3458A is, according to the data sheet of the manufacturer, measured at 1 mA current (at 100 Ω range) where the influence of the PC is insignificant.

Limits of Errors

Since the time constant is measured indirectly, the calculation of the safe limits of errors, as the maximum deviation of the device time constant from the true value is based on equations (1) and (2). The time constant of the standard is, using the measured values of R, L and C equal to 8.9639 ns. The limits of errors of the first term L/R in (1) are (0.3+0.3652+0.3284+0.007)%, which yields 1.0006 %. The second term in (2) is RC, and its limits of errors are (0.2104+0.007) %= 0.2174%.

For the equations including the difference as in (1), the overall safe limit of error is

$$G_{\%}=\pm\frac{|x_1G_{1\%}|+|x_2G_{2\%}|}{x_1-x_2} \quad (7)$$

where x_1 denotes first term (L/R) and x_2 denotes the second term (RC), while $G_{1\%}$ and $G_{2\%}$ are their accuracies [15].

For the measured R, L and C, the overall limit of errors is 1.264 % of the determined time constant or 113.30 ps.

This gives the limits of the phase angle error equal to 7.12 μrad or 0.00041° at 10 kHz, and the limits of the phase angle error equal to 71.19 μrad or 0.0041° at 100 kHz.

The minimum typical phase displacement of the Fluke A40B series precision current shunts (for shunts with nominal currents spanning from 1 mA to 100A) is below 0.006 ° at 10 kHz, and 0.060 ° at 100 kHz. At both frequencies, the limits of the phase angle errors of the time constant standard

is more than 10 times smaller of the expected measured phase angles, which makes the standard suitable for the determination of the phase angle displacements of such a type of the precision currents shunts.

Conclusions

A time constant standard, developed for the phase angle measurement of precision current shunts is developed and described, and its time constant has been determined. Based on a single circular loop, its construction is very simple and it gives accurate results in the frequency band of interest, e.g. for frequencies between 50 Hz and 100 kHz. Based on the power rating of 100 mW (in the air thermostat) and the DC resistance of the time constant standard, the maximum permissible current is 70 mA, which makes it suitable for the measurement of the phase angle error of shunts with the nominal current equal to 100 mA (and resistances typically equal to approximately 7 Ω). The correction of the resistance due to the power coefficient has to be taken into account. The time constant standard is also suitable for the measurement of the phase angle measurement of 10 mA shunts (with typical resistances equal to approximately 70 Ω), where the power rating is 2 mW. Using the step-up procedure [15] and the phase angle comparator, already developed at our laboratory [13], the phase angle displacement for the whole set of precision current shunts with nominal currents spanning from 1mA to 10 A can be determined.

Acknowledgment

This work was fully supported by Croatian Science Foundation under the project Metrological infrastructure for smart grid IP-2014-09-8826.

References

[1] D. Gibbings, “A design for resistors of calculable a.c./d.c. resistance ratio,” Proceedings of the Institution of Electrical Engineers, vol. 110, no. 2, pp. 335–347, February 1963.

[2] F. J. Wilkins and M. J. Swan, “Resistors having a calculable performance with frequency,” Proceedings of the Institution of Electrical Engineers, vol. 116, no. 2, pp. 318 - 324, 1969.

[3] S. Mašláň, M. Šíra; V. Nováková Zachovalová, J. Streit, „Simple resistance standard with calculable time constant,“ Conference on Precision Electromagnetic Measurements (CPEM 2016), Ottawa (ON), Canada, 2016, p. 1-2.

[4] Xianlin Pan, Jiangtao Zhang, Xuefeng Ma, Yang Gu, Wenfang Liu, Biao Wang, Zuliang Lu, and Deshi Zhang, »A Coaxial Time Constant Standard for the Determination of Phase Angle Errors of Current Shunts,« IEEE Trans. Instr. Meas, vol. 62, no. 1, January 2013, pp. 199-204.

[5] S. Svensson; K.-E. Rydler; V. Tarasso, »Improved Model and Phase-Angle Verification of Current Shunts for AC And Power Measurements,«

Conference on Precision Electromagnetic Measurements (CPEM 2004), London (UK), 2004, pp. 82-83,

[6] C. R. Paul, Inductance - Loop and Partial, John Wiley & Sons, 2010

[7] B.P. Kibble, G.H. Rayner, Coaxial AC Bridges, Adam Hilger, Bristol, 1984.

[8] H. W. Ott, Electromagnetic Compatibility Engineering, John Wiley & Sons, 2009

[9] L. Kefu, “Effect of a shield on the inductance of a conductor and its application to a compensated pulsed alternator,” in Fifth International Conference on Electrical Machines and Systems (ICEMS) , vol.2, 2001, pp. 1037-1041.

[10] J.P. Holman, Heat Transfer, McGraw-Hill, New York, 1997.

[11] Weinberg L. *Network Analysis and Synthesis*. McGraw-Hill;, New York, 1962.

[12] D. Deaver, N. Faulkner, Characterization of the Power Coefficient of AC and DC Current Shunts, 2010 NCSL International Workshop and Symposium, Providence, Rhode Island (USA)

[13] M. Dadić, P. Mostarac, R. Malarić, “Wiener Filtering for Real-Time DSP Compensation of Current Transformers over a Wide Frequency Range,” IEEE Transactions on Instrumentation and Measurement, vol. 66, no. 11, pp. 3023-3031, November 2017.

[14] Roman Malarić, Martin Dadić, Petar Mostarac:“D2.2. Report on designing, developing and testing current shunts“, Deliverable D.2.2. of Croatian Science Foundation project SMA-GRIMET, April 15th, 2016, 20 pp (in Croatian)

[15] V. Bego, Mjerenja u elektrotehnici, Tehnička knjiga, Zagreb, 1988.

[12] G. C. Bosco, M. Garcocz, K. Lind, U. Pogliano, G. Rietveld, V. Tarasso, B. Voljc, and V. N. Zachovalová, “Phase comparison of high current shunts up to 100 kHz,” IEEE Trans. Instrum. Meas., vol. 60, no. 7, pp. 2359–2365, Jul. 2011.

Journal of Energy

VOLUME 67 | 2018

journal homepage: http://journalofenergy.com/

Martin Dadić
University of Zagreb
Faculty of Electrical Engineering and Computing / FER
Zagreb, Croatia, martin.dadic@fer.hr

Tomislav Župan
KONČAR - Electrical Engineering Institute, Inc
Transformer Department, R&D Section
Zagreb, Croatia, tzupan@koncar-institut.hr

Gabrijel Kolar
University of Zagreb
Faculty of Electrical Engineering and Computing / FER
Zagreb, Croatia, gabrijel.kolar@fer.hr

Finite-Impulse-Response Modeling of Voltage Instrument Transformers Applicable for Fast Front Transients Simulations

Summary

This paper presents a method for Finite-Impulse-Response (FIR) modeling of voltage instrument transformers. The method is based on Wiener filtering and measurement of the transformer response in the frequency domain using a low frequency network analyzer. The proposed method allows, through digital filtering operation, an accurate simulation of the transformer response to transient excitation. Furthermore, the proposed approach to the modeling of the system function allows unequal spacing of the frequency samples. The linearity of the transformer is analyzed applying the Fourier analysis and different waveforms of the primary voltage, and methods for the model order selection, based on the generalized information criterion, are discussed and applied. The theoretical analysis is confirmed with measurements in time domain, using the recurrent surge generator.

Key words: transformer model, black-box, Wiener filetring, FIR filters, transfer function measurement, recurrent surge generator, lightning impulse

Introduction

Since transformers are typically constructed to work almost continuously during a period of forty years or more, they should be able to withstand both steady-state operation as well as possible transients in power grid. Most of the time the transformers are subjected to variations of less than 10% nominal voltage and 1% nominal frequency. All other types of excitation are considered as transients. Some of the typical causes of transients within the power grid are short circuits, switching operations, atmospheric discharges and almost any other changes within the system. Stresses that the insulation has to withstand can often have a great impact on design, performance and the overall price of the equipment. Standards typically classify transients into four groups (IEC 60071-2, 1996; IEEE 1313.2, 1999): low-frequency transients, slow front transients, fast front transients and very fast front transients. This paper focuses on the fast front transients which are normally aperiodic waves associated with near atmospheric discharges with a front time between 0.1 and 20 μs.

Due to various switching operations and atmospheric discharges, transformers are exposed to numerous overvoltages and have to be designed to correctly operate in those circumstances. The effects of transients are primarily visible on the transformer windings. The winding's ability to withstand overvoltages is determined by the shape of the transient signal, winding's geometry, characteristics of the insulation material and the overall condition of the winding including its age and past exposition to transients. A great number of transformer faults occur due to the insulation breakdown between turns of the winding. Steady state voltages under nominal grid frequency distribute linearly across the turns of the transformer winding and can be precisely determined. However, fast front transients usually lead to highly nonlinear voltage distribution. This often leads to high voltage stresses, especially at the beginning sections of the winding. Therefore, adequate mathematical models are needed to study the winding behavior at voltages with high frequency components.

Two main approaches to the transient modeling of transformers can be found in the literature published until today: the first one tries to accurately model the internal winding structure of transformers by modeling the capacitances, self- and mutual inductances and resistances. The second approach uses a black-box approach, where a model is built solely on the input/output data acquired during properly chosen experiments. In [1] the black box-approach uses bilinear transformation to build a discrete-time, z-domain model. In [2] a system identification approach is applied in a pole-zero sub-space modeling of distribution transformers intended primarily for the transformer fault-detection. This was done using frequency response analysis (FRA) measurements. In [3] a review of the applications of *z*-transform in electromagnetic transient simulations of power systems is given, with presented applications in transmission line modeling and power networks. In [4] a detailed overview of frequency-domain measurements methods for the validation of transformer models is given, alongside with methods for their rational-function approximation and re-

cursive convolution procedures for obtaining time-domain responses. In [5] a method for the black-box estimation of power transformers using the measurements performed with commercially available frequency-response-analyzers is presented. Since FRA equipment, dedicated for transformer measurements, measure input and output voltages grounded through matching resistors, a method based on two-independent measurements was developed that finally gives the admittance matrix, which can be used for the conversion to time-domain for no-load condition.

The main purpose of this paper is to provide a measurement procedure and a tool for the black-box estimation of conveying the fast or lightning transients of the voltage instrument transformers.

The approach is based on the frequency-domain measurements, and the measured response is used to build a discrete-time, Finite Impulse Response (FIR) transformer model. Once determined, FIR model allows, through the digital filtering operation, a very easy time-domain calculation of the system's response at any transient excitation. Through the digital filtering operation (closely related to the concept of recursive convolution [1]), the model output at any sample number n can be calculated by summation:

$$y(n) = w_0 x(n) + w_1 x(n-1) + ... + w_L x(n-L) \quad (1)$$

where L denotes model order, $x(n)$ is time-sampled input signal, and w_l are FIR model coefficients.

Wiener Filtering

Let a real input sequence x_k and a desired real output sequence d_k for k=0,1,2,… be given. The goal of Wiener filtering [6] is to find an Lth-order FIR filter (with filter coefficients w_0,….w_L)

$$H(z) = \sum_{r=0}^{L} w_r z^{-r} \quad , \quad (2)$$

which produces from the input, x_k, an estimate, d'_k , that minimizes the error between desired and modeled response.

This is a reduced-order approximation of the true impulse response of the system $H(\times)$. Here, w_r are filter coefficients, and z denotes the variable in the z-domain.

Its frequency response is characterized by

$$H(f) = \sum_{k=0}^{L} w_k e^{-jk2\pi fT} \quad 3)$$

where T denotes sample interval and f is the frequency.

The optimal solution of filter coefficients is obtained by solving the time-discrete Wiener-Hopf equation [6] .

$$\mathbf{Rw} = \mathbf{p} . \quad (4)$$

Here **R** denotes the autocorrelation matrix of the input, x_k

$$\mathbf{R} = \begin{bmatrix} r_{xx}(0) & r_{xx}(1) & ..... & r_{xx}(L) \\ r_{xx}(1) & r_{xx}(0) & ..... & r_{xx}(L\text{-}1) \\ . & & & \\ . & & & \\ r_{xx}(L) & r_{xx}(L\text{-}1) & & ..... \; r_{xx}(0) \end{bmatrix} \quad (5)$$

R is a symmetric Toeplitz matrix. The cross-correlation vector, **p**, between the desired response, d_k, and the input, x_k, reads as follows [6]:

$$\mathbf{p} = \begin{bmatrix} r_{dx}(0) & r_{dx}(1) & ..... & r_{dx}(L) \end{bmatrix}^{\mathrm{T}} \quad (6)$$

Further,

$$\mathbf{w} = \begin{bmatrix} w_0 & w_1 & ..... & w_L \end{bmatrix}^{\mathrm{T}} \quad (7)$$

denotes the coefficient vector of the Lth-order Wiener filter.

The Wiener-Hopf equation will not have a unique solution unless the equations are independent.

The transfer function to be modeled can be described in the frequency domain by a set of complex frequency samples:

$$H(\phi_l) = a_l \exp(j\theta_l) \quad , \quad l = [1, N]. \quad (8)$$

Here, defines magnitude response, defines phase response, and is the set of discrete frequencies for which the transfer function is defined. According to the Shannon sampling theorem, the sampling frequency f_s=1/T should be greater than twice the maximum frequency . Here, T denotes the sample interval.

For the system described by the transfer function (3), the input autocorrelation matrix, **R**, and the desired-to-input cross-correlation vector, **p**, are finally [7]:

$$\mathbf{R} = \frac{1}{2} \begin{bmatrix} \sum_{l=1}^{N} c_l^2 & \sum_{l=1}^{N} c_l^2 \cos 2\pi\phi_l T & ..... & \sum_{l=1}^{N} c_l^2 \cos 2L\pi\phi_l T \\ \sum_{l=1}^{N} c_l^2 \cos 2\pi\phi_l T & \sum_{l=1}^{N} c_l^2 & & \\ . & & & \\ . & & & \\ \sum_{l=1}^{N} c_l^2 \cos 2L\pi\phi_l T & . ..... & ..... & \sum_{l=1}^{N} c_l^2 \end{bmatrix} \quad (9)$$

$$\mathbf{p} = \frac{1}{2} \begin{bmatrix} \sum_{l=1}^{N} a_l c_l^2 \cos(\theta_l) \\ \sum_{l=1}^{N} a_l c_l^2 \cos(2\pi\phi_l T + \theta_l) \\ . \\ . \\ \sum_{l=1}^{N} a_l c_l^2 \cos(2L\pi\phi_l T + \theta_l) \end{bmatrix} \quad (10)$$

Here, denotes the sample interval, i.e. distance between samples, and c_l is a frequency-dependent positive weighting factor.

A Wiener-Hopf equation describes a system of linear equations that has a unique solution if **R** is a nonsingular matrix, i.e. if it is invertible [8]. In such a case, the system can generally be solved using Gaussian elimination. For some nonsingular matrices, the solution can also be found using certain factorization methods or iterative methods [9]. The Toeplitz structure of **R** allows application of Levinson's or Trench's algorithm as well [10].

A Wiener–Hopf equation (4) describes a system of linear equations that has a unique solution if **R** is a nonsingular matrix. Since every positive definite matrix is nonsingular [8], if the autocorrelation matrix is positive definite, it would be invertible. The matrix R is guaranteed to be a positive definite if the input signal $x(t)$ is spectrally rich, which will be fulfilled if there is at least half as many frequency components in $x(t)$ as there are coefficients in the Wiener filter [11], [12]. This condition will be easily satisfied with the increased number of the frequency samples in the measurements. In such a case, the solution of the system of equations (4) can be easily found using the MATLAB function *mldivide*, which performs Gaussian elimination for $n \times n$ square matrices and column vectors with n components. This technique was applied in all cases presented in the subsequent sections.

It was observed in our measurements, that measured transfer function, once converted from the frequency into time domain, may tend to be shifted "in advance". This does not cause any problem when dealing with the Fourier series, due to its time-periodicity. In system identification, it makes the impulse response of the target system noncausal. To include this shifted, "negative-time" portion of the system's impulse response in the model, it is wise to introduce a time delay in the desired response d_k for a fixed number of samples. In the frequency domain, it is performed by multiplication of the complex transfer function with , where n_0 denotes the delay in samples, T is sample interval and f is frequency. The possible causes of this phenomenon can be attributed to imperfections in the "through" calibration or measurement errors. It was also observed in radio-frequency measurements [13] and in FEM simulations [14] with the same solution. The modeling delay is discussed in more details in [15].

Measurement Set-Up

The measurements for the frequency-domain modeling of transformers can be divided in two approaches [4]:

— *voltage transfer measurements*
— *admittance matrix measurements*

For linear-time-invariant systems, the second approach gives a possibility of calculating the response for different loads (including no-load condition), while the voltage transfer measurement gives the response for the no-load condition or for a fixed load. Regarding the linearity, the model is assumed to be linear [5] since its experimental verification was carried out at low voltage in comparison to nominal voltages. This is generally the case for routine lightning-impulse testing of transformers.

The modeling procedure proposed in this paper applies the voltage transfer measurement, which was performed using a LF-RF network analyzer Keysight ENA 5061B and gain-phase test port. The LF option enables measurement of voltage transfer functions for frequencies spanning from 5 Hz to 30 MHz using the gain-phase port, while the input impedance can be switched between 50 Ω and 1 MΩ. The possibility of setting the high input impedance (1 MΩ) allows using high impedance oscilloscope probes with ratio 10:1 and 10 MΩ input impedance (shunted with the probe capacitance), which is approximately the same load applied with the oscilloscope probe in the time-domain measurements with the recurrent surge generator. Therefore, two oscilloscope probes Agilent 2862A (15 pF, 10 MΩ) were used in the measurement, and the "through" calibration of the analyzer was performed prior to measurements, which eliminates the influence of the probes on the measurement. This is especially important for the measurements in the MHz range. Use of high impedance (10 MΩ) probes further enhances the measurement in the MHz range, since using a 10:1 passive probes for oscilloscopes generally gives small input capacitance around 10 pF at the probe end. In this way, the load impedance is significantly increased when comparing to 1:1 passive probes. Similarly to general oscilloscope applications, it is an orthodox way for high impedance probing at higher frequencies [16]. The measurements were performed in the frequency range 5 Hz to 3 MHz, with the intermediate frequency bandwidth (IFBW) equal to 2 Hz. Use of low values of IFBW improves the measurement results, and in the same time slows the measurement process. For the same frequency range, increasing the IFBW to 100 Hz makes the measurement significantly faster, and does not the corrupt the results. The time-domain measurements were performed using a recurrent surge generator Haefely 481 and digital oscilloscope Tektronix DPO4054 equipped with voltage probes Tektronix P6139A (8 pF, 10MΩ). The FIR modeling was performed using a custom-made program in MATLAB, with sampling frequency equal to 6.004 MHz, which ensures, due to the Shannon sampling theorem the upper frequency limit of 3 MHz. To avoid non-causal response, a fixed modeling delay of 5 samples is introduced in measured transfer function.

The transformer is a voltage instrument transformer designed and manufactured in our laboratory for a digital sampling wattmeter application [17]. Its characteristics are as follows: nominal primary voltage is 230 V (RMS) at 50 Hz, class 1 according to IEC 61869-3, the targeted number of turns in the primary winding was N_p=1336 and N_s=45 in the secondary winding. The targeted maximum flux density at the primary voltage of 250 V (RMS) was set to 0.6 T, which ensures that the magnetic flux density is far bellow the saturation knee even at the primary voltage equal to 120% of its nominal value. The wire diameter in the secondary was chosen to be big enough to allow the secondary winding to be wound in a complete layer. Due to the high turn ratio, it was possible only with relatively big wire diameters, and the wire diameter of the secondary was chosen to be 1.2 mm. The wire diameter of the primary is 0.22 mm. In this way, each of the two sections of the primary consists of 4 complete layers. All layers were mutually isolated using the cellulose paper to allow easier assembling. The final number of turns was slightly different of the targeted, because all layers were wound completely to the edge of the former. The transformer core was a standard CM core CM85 (CM85b, older label SM85) core produced by Iskra Sistemi d.d. The CM cores consist of four core halves, with the coil former on the middle leg. To decrease leakage inductances and distributed capacitances, the sectionalized primary winding [18]-[21] with simple interleave was applied (Fig. 1). Due to the small burden (input impedance of the acquisition card NI-4461), the rated output of the VIT was chosen to be 1 VA at power factor 1. Fig. 2 presents the photo of the transformer.

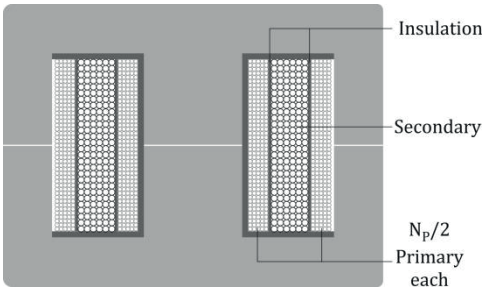

Figure 1. Configuration with simple interleave – sectionalized primary

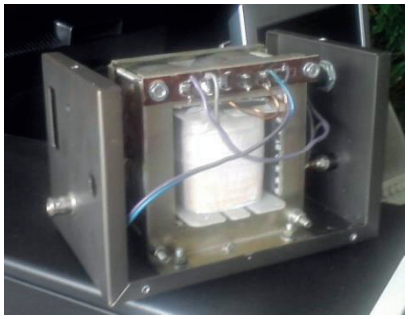

Figure 2. Transformer with the opened housing

Non-linearity analysis

Table I . Harmonic components of the secondary voltage for the single-tone stimulus

Harmonic order	1	2	3	4	5	6	7	8	9	10
Frequency (Hz)	50	100	150	200	250	300	350	400	450	500
Magnitude (%, compared to the fundamental)	100	0	0.8	0.7	0.3	0.1	0.4	0.1	0.1	0.2

The assumed linearity of the target system between primary and secondary voltages was further investigated applying the single-tone and multi-tone excitation and Fourier analysis. The nonlinear transfer function of a system generates the higher harmonic components at the output of the system, when the pure sine stimulus is applied. For the multi-tone excitation, the intermodulation occurs as well. The targeted maximum flux density in the transformer core, at the primary voltage of 250 V (RMS) was set in the design to 0.6 T, which ensures that the magnetic flux density is far below the saturation knee even at the primary voltage equal to 120% of its nominal value. Thus, for the nominal primary voltage and primary voltages lower than the nominal, it is expected that the relationship between primary and secondary voltage is nearly linear in the no-load condition. The measurement set-up for the non-linearity analysis was consisted of a Calmet C300 three phase power calibrator and tester and the power analyzer Chauvin-Arnoux CA8220. The sinusoidal distortion of the primary voltage, as declared by the calibrator manufacturer (Calmet) is 0.05 %.

In the first set of the measurements, the single-tone voltage was applied at the primary, where the primary voltage was nominal (e.g. 230 V, 50 Hz). At the secondary the RMS values of the first 10 harmonics were measured, as well as the total harmonic distortion in relation to the fundamental (THD_F) for the first 50 harmonic components. THD_F is expressed as

$$\mathrm{THD_F} = \frac{\sqrt{I_2^2 + I_3^2 + \ldots\ldots + I_n^2}}{I_1}, \tag{11}$$

where I_1 denotes magnitude of the fundamental harmonic, and I_2 to I_n denote magnitudes of the higher harmonics. The measured THD_F of the secondary voltage was 1.5 %, while the RMS values of the first 10 harmonic components, in percentages compared to the fundamental are systemized in the Table I.

For the two-tone excitation, the further insight in the generation of the intermodulation components can be obtained using the following analysis: Suppose that the non-linear transcharacteristic of the system can be

expanded about the operating point by mean of power series

$$e_o = a_0 + a_1 e_i + a_2 e_i^2 + a_3 e_i^3 \tag{12}$$

where e_i and e_o are the alternating parts of the input and output voltages. If the input signal is composed of two cosines with radian frequencies p and q,

$$e_i = P\cos(pt) + Q\cos(qt) \tag{13}$$(13)

the harmonic distortion and intermodulation components are [22]:

$$\begin{aligned} e_o = &\left(\frac{1}{2}a_2P^2 + \frac{1}{2}a_2Q^2\right) + \left(a_1P + \frac{3}{4}a_3P^3 + \frac{3}{2}a_3PQ^2\right)\cos(pt) \\ &+ \left(a_1Q + \frac{3}{4}a_3Q^3 + \frac{3}{2}a_3P^2Q\right)\cos(qt) \\ &+ \frac{1}{2}a_2P^2\cos(2pt) + \frac{1}{2}a_2Q^2\cos(2qt) \\ &+ \frac{1}{4}a_3P^3\cos(3pt) + \frac{1}{4}a_3Q^3\cos(3qt) \\ &+ a_2PQ[\cos(p+q)t + \cos(p-q)t] \\ &+ \frac{3}{4}a_3P^2Q[\cos(2p+q)t + \cos(2p-q)t] \end{aligned} \tag{14}$$

More generally, if the input signal is consisted of the two sine components, it is expected that the non-linear transfer function (transcharacteristic) generates both the higher harmonic components of each input sine (with the radian frequencies 2p, 3p ,,, 2q, 3q, etc.) and the intermodulation components with the radian frequencies p+q , p-q , 2p+q , 2p-q , etc. For the input voltage consisted of two sine tones with the frequencies equal to 50 and 100 Hz, it is this expected that at the output of the system the second-order summation component with the frequency equal to 150 Hz is certainly present.

Figure 3. Two-tone waveform

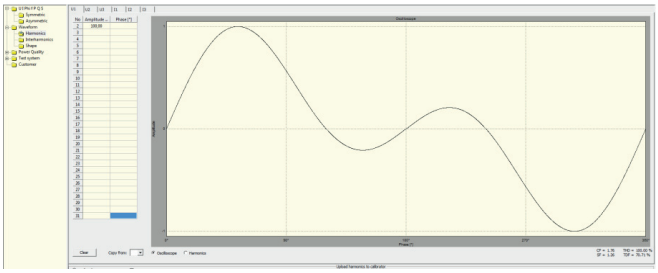

In the second set of measurements, the primary voltage generated by the calibrator was consisted of two sine tones with the equal magnitudes and frequencies 50 Hz and 100 Hz. Fig. 3 presents the waveform of the primary voltage. The RMS value of this composite voltage was set again to 230 V RMS. In the Table II, the harmonic analysis of the secondary voltage is presented.

Table II . Harmonic components of the secondary voltage for the two-tone stimulus

Harmonic order	1	2	3	4	5	6	7	8	9	10
Frequency (Hz)	50	100	150	200	250	300	350	400	450	500
Magnitude (%, compared to the fundamental)	100	99.5	0.7	0.8	0.4	0.2	0.4	0.4	0.4	0.4

It can be seen from the Tables I and II, that the magnitudes of the generated higher harmonic components are negligible, compared to the fundamental and that the THD_F is low at the secondary for a single-tone excitation. Moreover, for the two-tone excitation, the magnitude of the summation tone (150 Hz) is equal to its relative magnitude for the single-tone excitation, which further approves that the intermodulation components are negligible, and that the system can be regarded as linear. It should be pointed that the whole analysis is presented for the primary and secondary voltages, which are the measured parameters for both FRA and impulse response analysis. The possibly non-sinusoidal magnetization current therefore does not influence the assumed linearity of the relationship between the primary and secondary voltages.

Results

Standard lightning impulse (LI)

The first set of time-domain measurements was performed with the standard lightning impulse (1,2 μs/50 μs) according to IEC 60060-1. The sample interval of the oscilloscope in the time-domain measurements with the recurrent surge generator was 10 ns. To match the exciting signal with the sample period of the FIR model (e.g. = 0.16656 μs), the LI was resampled using MATLAB function *interp*. The filter order was L=300 (i.e. the overall number of the coefficients was 301), and the modeling delay was 5 samples. The frequency-dependent positive weighting factors c_l were all set to 1. Fig. 4 presents the frequency response (magnitude) of the model, compared to the frequency domain measurements using the network analyzer. Fig. 5 depicts the measured input voltage, while Fig. 6 presents the simulated response. The simulated response is the result of the digital filtering operation using the estimated FIR model and measured excitation. Fig. 7 gives the comparison of the simulated and measured response in the time-domain. The simulated time-domain response is shifted “in left” for 5 samples, to compensate the modeling delay.

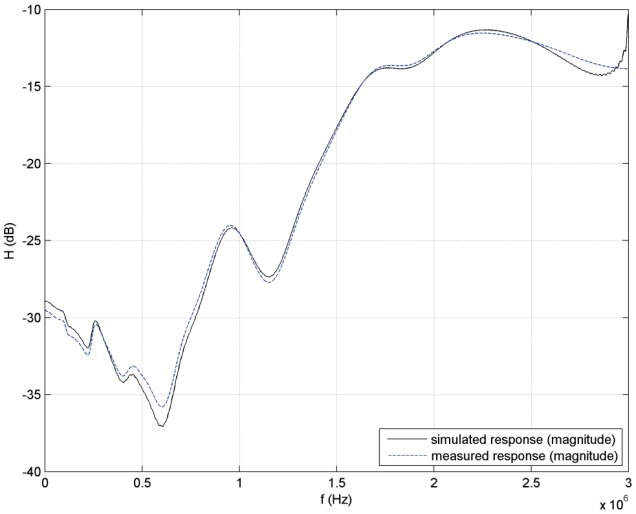

Figure 4. Comparison of measured and modeled transfer function - magnitude

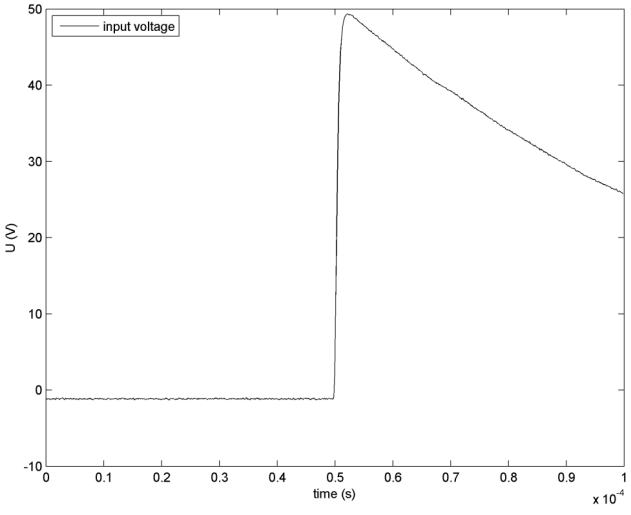

Figure 5. Measured excitation – full wave

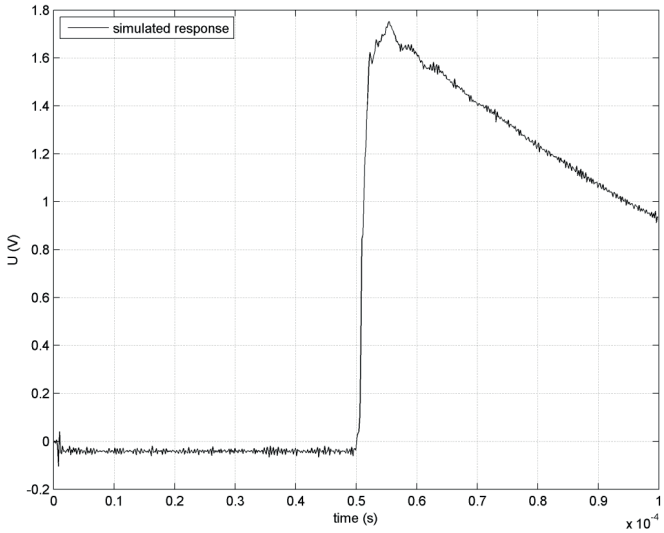

Figure 6. Simulated response – full wave

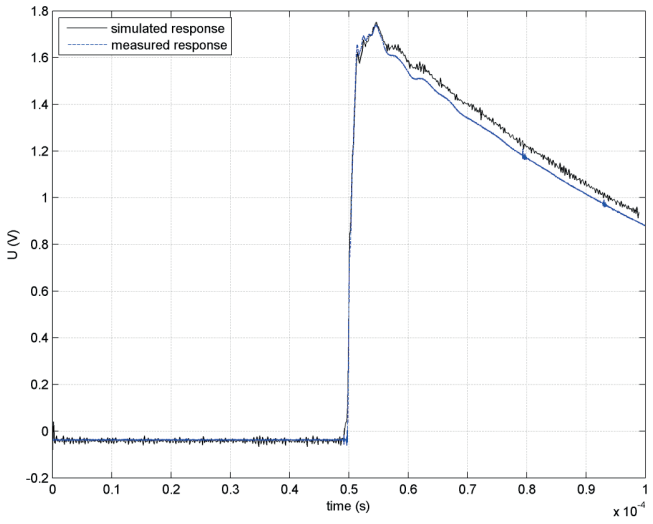

Figure 7. Comparison of measured and simulated response for the full wave excitation

Lightning impulse chopped on the front (LI-CF)

The second set of time-domain measurements was performed using the lightning impulse chopped on the front according to IEC 60060-1. All settings were the same as in (A), except the sample interval of the oscilloscope, which was 4 ns. Fig. 8 depicts the measured input voltage, while Fig. 9 gives the comparison of the simulated and measured response in the time-domain. The simulated time-domain response is shifted “in left” for 5 samples, to compensate the modeling delay.

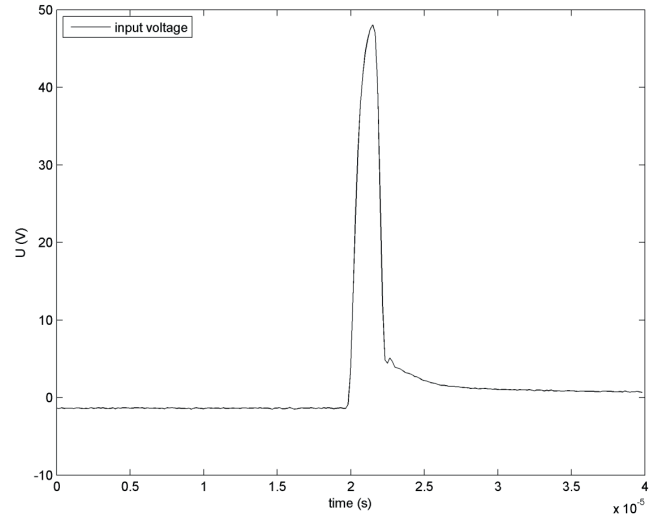

Figure 8. Measured excitation – chopped wave (CF)

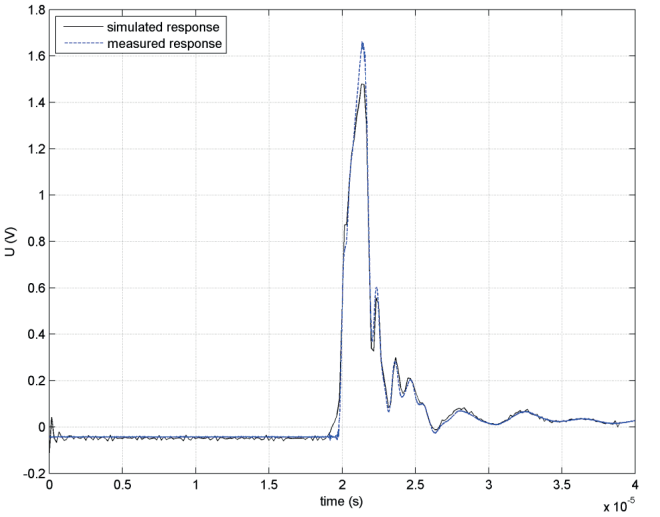

Figure 9. Comparison of measured and simulated response for the chopped wave excitation (CF)

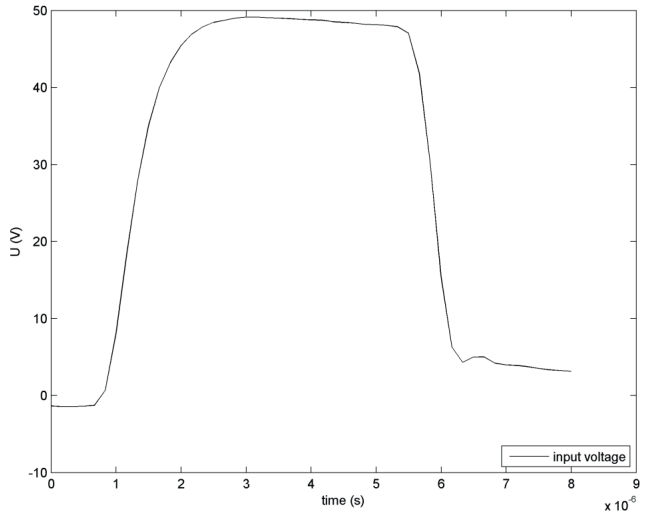

Fig. 10. Measured excitation – chopped wave (CT)

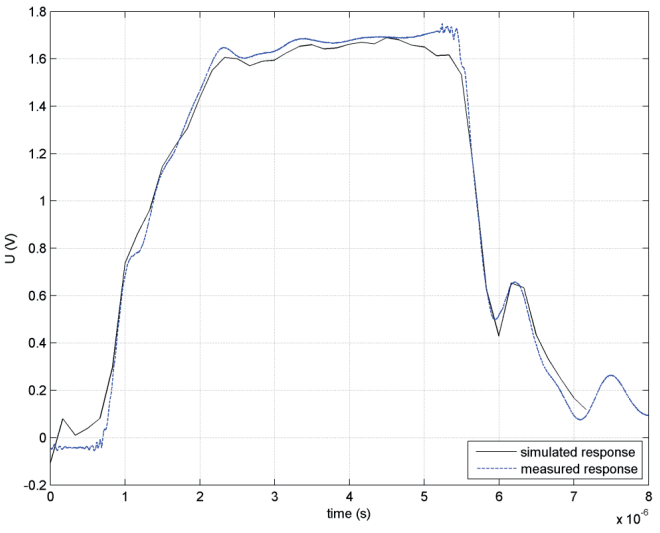

Fig. 11. Comparison of measured and simulated response for the chopped wave excitation (CT)

Lightning impulse chopped on the tail (LI-CT)

The third set of time-domain measurements was performed using the lightning impulse chopped on the tail according to IEC 60060-1, with chopping time of around 5 μs. All settings were the same as in (A), except the sample interval of the oscilloscope, which was 0.8 ns. Fig. 10 depicts the measured input voltage, while Fig. 11 gives the comparison of the simulated and measured response in the time-domain. The simulated time-domain response is shifted "in left" for 5 samples, to compensate the modeling delay.

FIlter Order Selection

With the increase of the filter order, a better fit of the model and the measurements is achieved. As the trade-off between complexity of the model and the better fit to the data, different order-selection criteria can be applied. Several order selection criteria [23-30] can be systemized as generalized information criterion (GIC). It can be approximated using the variance estimate

$$\hat{\sigma}^2 = \frac{1}{N}\|y - \hat{y}\|^2 \tag{16}$$

as

$$GIC = \text{constant} + N \ln \hat{\sigma}^2 + \nu m \tag{17}$$

where N denotes the number of samples in the data vector, m denotes the number of estimated parameters andis the penalty factor for the increase of the model size. The model order m is selected as the minimum of GIC for the proposed model orders between 0 and some maximum candidate. For finite values of N, the corrected Akaike criterion (AICc):

$$\nu = \frac{2N}{N - m - 1} \tag{18}$$

is suitable for the order-selection, with a smaller risk of overfitting compared to the Akaike criterion (AIC). AICc was already applied as the order-selection criteria in the impulse response modeling of the voltage instrument transformers [31].

The example of order-selection based on AICc is performed using model orders spanning from 1 to 1598, where the variance estimate (16) is calculated as the Euclidean distance between measured and calculated frequency response, for the frequencies determined by the data set of the measurement. Here, N is the number of frequency samples in the measurements. The adequate filter order according to AICc appeared to be L_{AICc}=71. Fig. 12 depicts the comparison of the simulated and measured response in the time-domain for the lightning impulse chopped on the tail (LI-CT). The simulated time-domain response is shifted "in left" for 5 samples, to compensate the modeling delay. The routine for calculation of AICc was programmed in MATLAB by the authors.

Figure 12. Comparison of measured and simulated response for the chopped wave

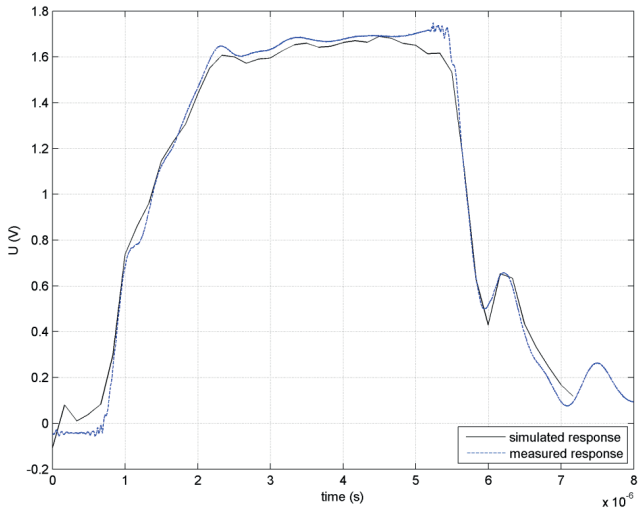

excitation (CT) – filter order is selected according to AICc

Conclusions

This paper describes a novel approach in the modeling of transformers, suitable for time-domain simulation of their response during the fast transients. On the basis of the frequency-domain measurements using a low-frequency network analyzer with the gain-phase test port, the z-domain, finite impulse response (FIR) model of the system function is built. The proposed technique is based on Wiener filtering and the frequency domain approach in the system identification. Since the proposed technique applies finite impulse response filtering, the z-domain model of the transformer is absolutely stable. Such a model, being a digital FIR filter, allows easy computation of the response of the system to various exciting voltages without a need for the measurements in the time-domain to be performed again for each transient excitation. Furthermore, Wiener modeling of the system function allows unequal spacing of the frequency samples. This gives the possibility of greater accuracy of the modeling in the frequency range where the magnitude or phase response of the system varies greatly. The linearity of the transformer is confirmed applying the Fourier analysis and different waveforms of the primary voltage, and methods for the model order selection, based on the generalized information criterion are discussed and applied. The theoretical analysis is confirmed with measurements in time domain, using the recurrent surge generator, and a very good matching is achieved between the simulated and measured time-domain responses for several different transient excitations.

Acknowledgment

This work has been fully supported by the Croatian Science Foundation under the project number IP-2013-1118.

References

[1] Q. Su, R.E. James, D. Sutanto, "A z-transform model of transformers for the study of electromagnetic transients in power systems," IEEE Transactions on Power Systems, vol. 5, no. 1, February 1990, pp. 27-32.

[2] Akcay, S. Islam, B. Ninnes, "Identification of power transformer models from frequency response data: A case study," Signal Processing, 68(1998), pp. 307-315.

[3] T. Noda, A. Ramirez, "z-Transform-Based Methods for Electromagnetic Transient Simulations," IEEE Transactions on Power Delivery, vol. 22, no. 3, 2007, pp. 1799-1805.

[4] B. Gustavsen, A. Portillo, R. Ronchi, A. Mjelve, "Measurements for validation of manufacturer's white-box transformer models," 4th International Colloquium "Transformer Research and Asset Management", Procedia Engineering 202 (2017), pp. 240-250.

[5] D. Filipović-Grčić, B. Filipović-Grčić, I. Uglešić, "High-Frequency Model of the Power Transformer Based on Frequency-Response Measurements," IEEE Transactions on Power Delivery, vol. 30, no. 1, February 2015, pp. 34-42.

[6] S.D. Stearns, R.A. David, Signal Processing Algorithms, Englewood Cliffs: Prentice Hall, 1988.

[7] B. Widrow, S.D. Stearns, Adaptive Signal Processing, Upper Saddle River: Prentice Hall, 1985.

[8] R.A. Horn, C.R. Johnson, Matrix Analysis, Cambridge: Cambridge University Press, 1990.

[9] J.E. Gentle, Numerical Linear Algebra for Applications in Statistics, Springer, 1998.

[10] S.D. Stearns, Digital Signal Processing with Examples in MATLAB, Boca Raton: CRC Press, 2003.

[11] G. C. Goodwin and K. S. Sin, Adaptive Filtering: Prediction and Control. Englewood Cliffs, NJ, USA: Prentice-Hall, 1984.

[12] P. A. Nelson and S. J. Elliott, Active Control of Sound. London, U.K.: Academic, 1992.

[13] Zentner, R.; Dadić, M.; Šipuš, Z.; Bartolić, J.: Time Domain Analysis of Mutual Coupling Measurements between Stacked Patches. ICECom 2003 Conference Proceedings / 17th International Conference on Applied Electromagnetics and Communications. Dubrovnik 2003, 370-373.

[14] Dadić M, Vasić D, Bilas V. A system identification approach to the modelling of pulsed eddy-current systems. NDT & E International 2005;38(2): 107-111.

[15] Martin Dadić, Petar Mostarac, and Roman Malarić, Wiener Filtering for Real-Time DSP Compensation of Current Transformers over a Wide

Frequency Range, IEEE Transactions on Instrumentation and Measurement, Vol. 66, No. 11, Nov. 2017, pp. 3023-3031.

[16] Keysight Technologies: Measuring Frequency Response with the Keysight E5061B LF-RF Network Analyzer, Application Note, http://literature.cdn-keysight.com/litweb/pdf/5990-5578EN.pdf (accessed September 18, 2018)

[17] Dadić, Martin; Petrović, Karlo; Malarić, Roman. FEM analysis and design of a voltage instrument transformer for digital sampling wattmeter: MIPRO 2017 Proceedings, Opatija : MIPRO, 2017. pp. 174-178.

[18] C. Wm. T. McLyman, Transformer and Inductor Design Handbook, 4th Edition, CRC Press, 2011.

[19] G. Koehler, "The Design of Transformers for Audio-Frequency Amplifiers with Preassigned Characteristics," Proceedings of the IRE, vol. 16, no. 12, pp. 1742-1770, 1928.

[20] T. Jelaković, Transformatori i prigušnice, Biblioteka časopisa „Elektrotehničar", Zagreb 1952.

[21] F. E. Terman, Radio Engineer's Handbook, McGraw, 1943.

[22] Arguimbau LB. *Vacuum-Tube Circuits and Transistors*. Wiley: New York, 1956.

[23] Stoica P, Selén Y. A review of information criterion rules. IEEE Signal Processing Magazine. vol. 21, no. 4, 2004, pp.36-47.

[24] Selén Y, Gudmundson E, Stoica P. An Approach to Sparse Model Selection and Averaging. IMTC 2006 – Instrumentation and Measurement Technology Conference. Sorento Italy 24-27 April 2006, pp.113-116.

[25] Broersen PMT. Finite Sample Criteria for Autoregressive Order Selection. IEEE Transactions on Signal Processing. Vol.48, no.12, 2000, pp.3550-3558.

[26] Tjärnström F, Ljung L. L_2 model reduction and variance reduction. Automatica, vol. 38, 2002, pp.1517-1530.

[27] de Waele S, Broersen P.M.T. Order Selection for Vector Autoregressive Models. IEEE Transactions on Signal Processing, vol. 51, no.2, 2003, pp. 427-433.

[28] Söderström T, Stoica P, Friedlander B. An indirect prediction error method for system identification. Automatica, vol.27, no.1, 1991, pp.183-188.

[29] Young P, Jakeman A, McMurtries R. An instrumental variable method for model order identification. Automatica, vol. 16, 1980, pp. 281-294.

[30] Djurić PM. Asymptotic MAP criteria for model selection. IEEE Transactions on Signal Processing, vol. 46, no. 10, 1998, pp.2726-2735.

[31] Dadić M, Keitoue S., Malarić R., Gazivoda S. FIR modeling of voltage instrument transformers with iron core for the study of fast transients, Measurement, vol. 43, no. 10, 2010, pp. 1404–1415

Journal of Energy

VOLUME 67 | 2018

journal homepage: http://journalofenergy.com/

Jure Konjevod
University of Zagreb
Faculty of Electrical Engineering and Computing / FER
Zagreb, Croatia, jure.konjevod@fer.hr

Roman Malarić
University of Zagreb
Faculty of Electrical Engineering and Computing / FER
Zagreb, Croatia, roman.malaric@fer.hr

Martin Dadić
University of Zagreb
Faculty of Electrical Engineering and Computing / FER
Zagreb, Croatia, martin.dadic@fer.hr

Ivica Kunšt
University of Zagreb
Faculty of Electrical Engineering and Computing / FER
Zagreb, Croatia, ivica.kunst@fer.hr

Hrvoje Hegeduš
University of Zagreb
Faculty of Electrical Engineering and Computing / FER
Zagreb, Croatia, hrvoje.hegedus@fer.hr

AC-DC Characterization of Coaxial Current Shunts and Application of the Shunt in the Digital Sampling Wattmeter

Summary

The purpose of this paper is to give a review of ac-dc characterization of the current shunts and application of the current shunt (nominal current 1A) within the digital sampling wattmeter. It is described the ac-dc transfer difference measurement of six cage type ac shunts from 10 mA up to 10 A using step-up measurement procedure. Furthermore, the substantial part of the measurement setup is fast switching system which is also described in detail. For the purpose of measurement procedure, the application is developed in LabVIEW and whole process is fully automatized. Obtained results are analyzed and shown on graphs. This paper is extended version of two papers: [1] and [2] which are presented on 1st International Colloquium on Smart Grid Metrology. Thus, paper is extended with presented application of the shunt 1 A in the digital sampling wattmeter.

Key words: current shunt, step-up procedure, thermal voltage converter, automated measurement procedure, digital sampling wattmeter

Nomenclature

$V_{AC}(rms)$	*root-mean square value of the sinusoidal voltage*
δ_{AC-DC}	*ac-dc difference*
V_{DC}	*dc voltage*
V_{AC}	*ac voltage*
E_{DC}	*output EMF of the thermocouple when the dc voltage is applied*
E_{AC}	*output EMF of the thermocouple when the ac voltage is applied*
Δ_0	*relative error between E_{AC} and E_{DC}*
V_{DC}^S	*output voltage of the referent standard when the dc voltage is applied*
V_{AC}^S	*output voltage of the referent standard when the ac voltage is applied*
V_{DC}^X	*output voltage of the unit under test when the dc voltage is applied*
V_{AC}^X	*output voltage of the unit under test when the ac voltage is applied*
k^x	*exponent of the thermal voltage converter (TVC) response (for the referent standard)*
k^S	*exponent of the thermal voltage converter (TVC) response (for the unit under test)*

J. Konjevod, R. Malarić, M. Dadić, I. Kunšt, H. Hegeduš, AC-DC Characterization of Coaxial Current Shunts and Application of the Shunt in the Digital Sampling Wattmeter, vol. 67 (2018), Special Issue, p. 15–18

Introduction

Resistive shunts are used as current transducers which transfer current into voltage for the purpose of current and power measurements. Such system for electric power measurement is digital sampling wattmeter. Transducers used as reference standards for these calibrations must be stable and insensitive to temperature and signal levels and have a small ac-dc transfer difference at frequencies up to 100 kHz [3]. The shunts which are used in national metrology laboratories to satisfy required parameters and also analyzed in this paper are cage type designed similar to SIQ AC shunts [4], and are fabricated using double-sided FR4 fiberglass-epoxy PCB material, equipped with N-type connectors, and constructed with three circular PCB elements, crossbars and resistors. Thermal converters are the most accurate standards for the transfer of alternating current to the equivalent dc quantities [5]. A special type of thermal converter is used in this measurement and it is planar multi junction thermal converter (PMJTC (90 Ω)). It is designed and assembled at the IPHT (*Institute of Photonic Technology*) in Jena, Germany. Switching between ac and dc source with the shortest possible interruption of the input voltage is a prerequisite to achieve constant heating conditions in the PMJTCs. Since, the switching time must be small compared to the thermal time constant of the PMJTCs [6]. Consequently, each thermal AC-DC voltage transfer measurement system requires a device which performs fast switching of the input of the thermal voltage converter (TVC) between AC and DC calibrator outputs. There are no commercially available switches on the market, which could be directly implemented in the AC-DC transfer [7].

AC-DC Transfer Difference

Ac-dc transfer difference measurement system

Generally, the ac voltage is defined by the root-mean square (rms) value of the sinusoidal waveform;

$$V_{AC}(rms) = \sqrt{\frac{1}{T}\int_0^T \left(V(t)\right)^2 dt} \tag{1}$$

According to the definition, it is possible to compare the ac voltage with the dc by way of the electrical power. In the thermal method, dc and ac voltage are alternately applied to the heater of a thermal converter. Then the amounts of joule heating are compared by measuring the temperature of the heater by a thermocouple. By applying ac and both polarities of dc in measurement sequence, and measuring the thermocouple output, the conventional definition of ac-dc difference is [1]:

$$\delta_{AC-DC} = \frac{V_{AC}-V_{DC}}{V_{DC}}\Big|_{E_{AC}=E_{DC}} \tag{2}$$

Here the quantities and represent the output EMFs of the thermocouple when the dc voltage and the ac voltage are applied to a thermal converter. If a thermal converter is ideal then [8]. The current shunt ac-dc transfer measurement system consists of following components: dc and ac voltage source, power amplifier, relay box, T-connector for serial connection of the shunts, two control digital multimeters (DMMs) and two DMMs (HP 3458A) for measuring. Detailed connections of current T-connector and coaxial cables as part of whole measuring system are shown in Fig.1 and whole measurement setup is shown in Fig.2. [1].

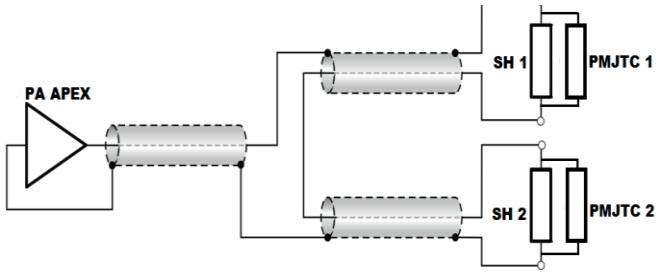

Figure 1. Connections in measuring system for AC-DC transfer difference of current shunts [1]

The software for the measurement setup was programmed in LabVIEW programming environment. Output voltages of thermal converters (PMJTCs) are simultaneously sampled using triggering function. Thus, acquired voltages are processed with developed LabVIEW application. AC-DC transfer difference of shunts (10 mA to 10 A) have been measured according to scheme depicted on Fig. 2. Calibrator Transmille 3050A is used as a DC source. Same device is used as power source in the digital sampling wattmeter. Arbitrary/function generator Tektronix AFG 3021B is used as AC source for AC-DC transfer measurement.

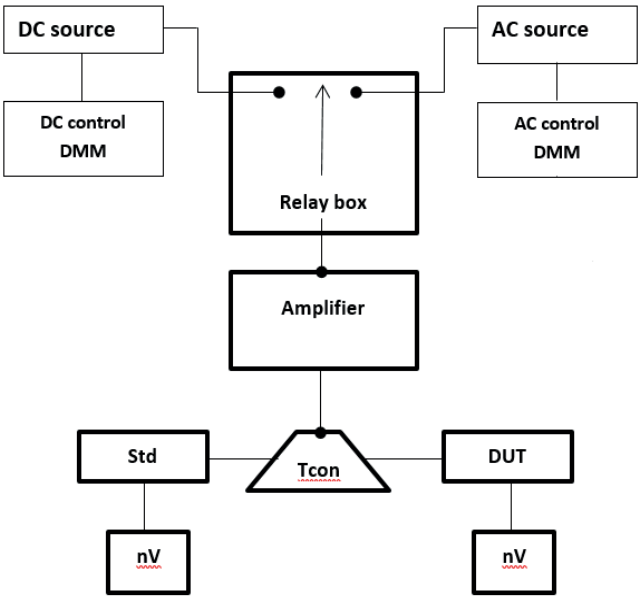

Figure 2. Connections in measuring system for AC-DC transfer difference of current shunts [1]

Switch used in the ac-dc transfer difference measurement system

The switch consists of three units. The control unit (NI USB-6008 and UL-N2803A Darlington Transistor Arrays) is outside the relay box which houses four relays and holds the input and output connectors. Input and output connectors are used to connect ac source, dc source, digital multimeter and load. So, relays are separated from electronic device because of their thermal interference. During the measurements, the relay unit is therefore free of any electrical signals on the relay driving side. This is important to obtain both a low noise level and a good thermal stability. Also, in spite the fact that relays are latch type, to be sure that each relay works on the same temperature, all relays are mounted on the copper plate with thermal paste and relays are mutually connected. Besides, these relays have been chosen as a compromise between number of mutual connections, number of connections with other components and length of operational and release time. All connections between relays in relay box, as well as out of the box, is shown in Fig.3. Further, the whole relay box and manual PCB design for relay control were assembled at our laboratory and have been used in ac-dc difference measurement application. The operating time and release time indicate the time required for each contact to close after the voltage has been applied to or removed from the coil. However, because the relay has a mechanical structure, a bounce state exists at the end of the operating and release times. Moreover, for the purpose of ac-dc transfer measurement, whole measurement process is automatized using LabVIEW and relay box performs measurement sequence: ac, dc+, ac, dc-, ac [2]. Thus, used relay box enables required conditions for ac-dc transfer measurement.

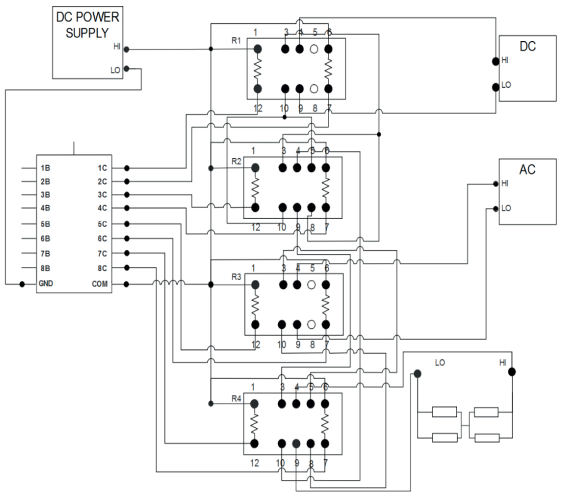

Figure 3. Mutual connections of relays in relay box and outer connections with other components [2]

J. Konjevod, R. Malarić, M. Dadić, I. Kunšt, H. Hegeduš, AC-DC Characterization of Coaxial Current Shunts and Application of the Shunt in the Digital Sampling Wattmeter, vol. 67 (2018), Special Issue, p. 15–18

Ac-dc transfer difference measurement procedure

The software program developed in LabVIEW sets the initial voltage and frequency of ac source and voltage of dc source. After that it has been waiting for heating of current shunts and stabilization. The frequency of the output voltage waveform from arbitrary function generator is swept across a specified range (from 50 Hz to 100 kHz). "Step-up" measurement procedure which is presented in [9] has been used for AC-DC transfer difference measurement and shown in Fig. 3. Voltage signals from DC and AC source are amplified with power amplifier Apex Eval 57 R-A with gain factor of 10. Digital multimeters HP3458A are used as nanovoltmeters (100 mV input range) to measure voltage outputs from PMJTC because its voltage output has enough large value to measure without special nanovoltmeters. Voltage on the AC source is set to be constant during the AC-DC transfer measurement of a shunt and voltage on DC source has been adjusted by proportional gain of PID regulator which is also programmed in LabVIEW application. Each measurement sequence has been performed and measurement result has been taken into account only if it satisfies next condition [1]:

$$\Delta_0 = \frac{E_{AC}-E_{DC}}{E_{DC}} \leq 50\ \mu V/V \quad (3)$$

,

where and represent the output EMFs of the thermocouple on the referent standard channel. Time delay is 60 seconds in all the steps of measurement sequence. AC-DC transfer measurement has been performed for DC and next frequency points: 50, 100, 1000, 10000, 20000, 50000 and 100000 Hz.

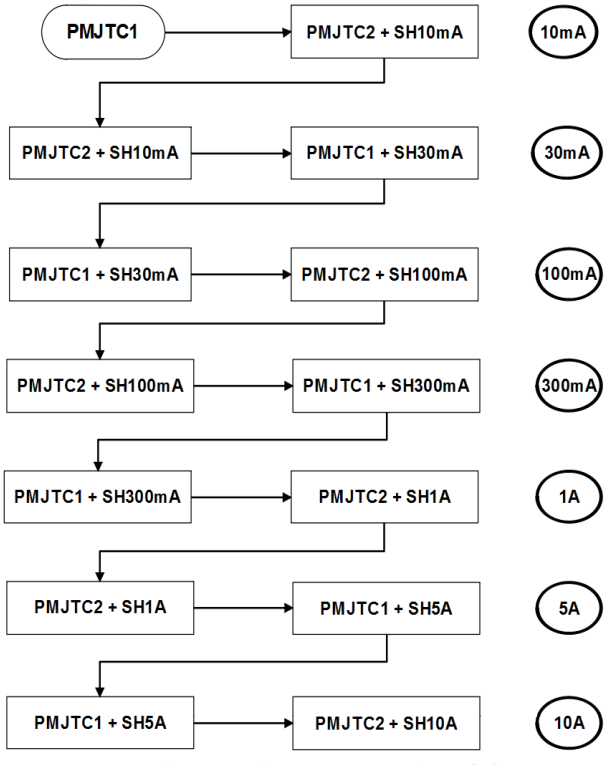

Figure 4. Step up procedure [1]

When two shunts (with PMJTCs in parallel with each of the shunt) "s" and "x" have been compared, difference between two ac-dc transfers can be obtained from next two expressions [1]:

$$\delta = \delta_X - \delta_S \quad (4)$$

i.e.,

$$\delta = \frac{V_{DC}^X - V_{AC}^X}{k^X V_{DC}^X} - \frac{V_{DC}^S - V_{AC}^S}{k^S V_{DC}^S} \quad (5)$$

, where V_{DC}^S i V_{AC}^S are output voltages of the referent standard (shunt and PMJTC in parallel combination) when dc and ac is applied. V_{DC}^X i V_{AC}^X are output voltages of the unknown combination (shunt and PMJTC in parallel combination).

k^x i k^S are the exponents of the thermal voltage converter (TVC) response, with typically k = 2 for PMJTCs [10].

Considering preformed measurement procedure and related measurement sequence, following expressions are applied [1]:

$$V_{DC}^S = \frac{V_{DC+}^S + V_{DC-}^S}{2},\ V_{AC}^S = \frac{V_{AC_1}^S + V_{AC_2}^S}{2}, \quad (6)$$

$$V_{DC}^X = \frac{V_{DC+}^X + V_{DC-}^X}{2},\ V_{AC}^X = \frac{V_{AC_1}^X + V_{AC_2}^X}{2}$$

Since the ac-dc difference of the reference standard is known, then the ac-dc difference of the unknown can be obtained from the next expression [10]:

$$\delta_X = \delta_S + \frac{V_{DC}^X - V_{AC}^X}{k^X V_{DC}^X} - \frac{V_{DC}^S - V_{AC}^S}{k^S V_{DC}^S} \quad (7)$$

Thus, when condition (3) is fulfilled, ten measurement results has been taken and their mean is calculated [1]:

$$\delta_X = \frac{\sum_{i=1}^{10} \delta_i^x}{10} \quad (8)$$

Results and Discussion

Ac-dc transfer difference results

Graph shown in Fig. 5. represents values of ac-dc differences for all shunts, values are overlapped and visible as one line. So, all shunts have almost the same trend to the frequency of 20 kHz.

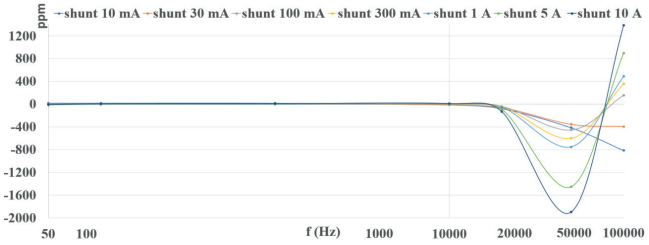

Figure 5. AC-DC transfer difference for shunts with nominal current from 10 mA to 10A for whole frequency range (Linear approximation) [1]

Further, the graph in Fig.6. shows ac-dc difference of shunt (nominal current 1A) that is used as component in digital sampling wattmeter.

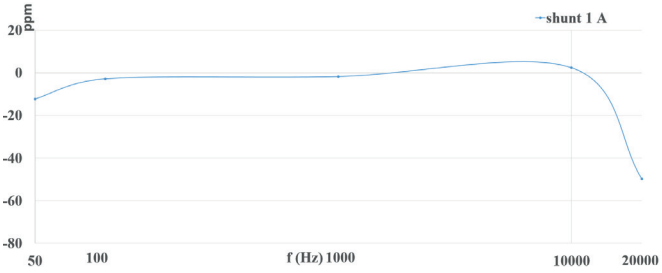

Figure 6. AC-DC transfer difference for shunt with nominal current of 1 A for frequency range from 50 Hz to 20 kHz (Linear approximation)

Digital sampling wattmeter results

Current signal from power source is converted into voltage signal via current shunt. Used shunt has nominal current of 1 A and its ac-dc transfer characteristics is shown in Fig. 6. When nominal current of shunt is applied at the input, obtained voltage amplitude at its output is 1 V. Also, voltage signal is transformed from high level of 560 V to 10 V via resistive voltage divider developed at the Faculty of electrical engineering and computing [11]. Both signals are sampled with digital multimeters HP3458A in master-slave configuration. Output voltage of the current shunt is sampled with slave DMM over four values of frequency and results are shown on Fig. 7. Output voltage of the resistive voltage divider is sampled with the master DMM (Fig. 8.). Maximum signal frequency of calibrator Transmille 3050A when used as power source (i.e. in power mode) is 400 Hz.

J. Konjevod, R. Malarić, M. Dadić, I. Kunšt, H. Hegeduš, AC-DC Characterization of Coaxial Current Shunts and Application of the Shunt in the Digital Sampling Wattmeter, vol. 67 (2018), Special Issue, p. 15–18

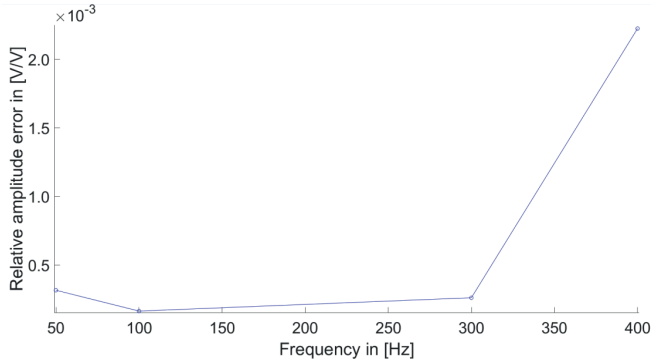

Figure 7. Relative amplitude error of voltage for current shunt with nominal current of 1 A

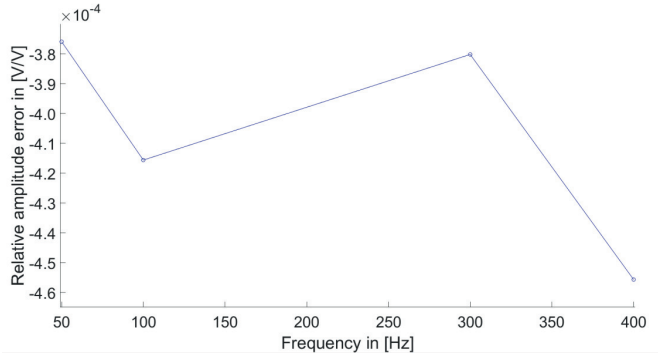

Figure 8. Relative amplitude error of voltage for resistive voltage divider

Samples are acquired in LabVIEW and processed using interpolated DFT algorithm. Interpolated DFT algorithm calculates amplitude, phase and frequency when sine wave signal is noncoherently sampled, a non-integer number of signal periods is contained in the sampled record. Also, interpolated DFT algorithm fight this inherent leakage using time-domain windowing, which effectively reduces the leakage, but at the same time increases the estimated standard deviation due to noise contained in the sampled record [12].

Conclusion

After analyzing obtained results, it can be concluded that relative amplitude error of current shunt is in the same order as the relative amplitude error of voltage divider. But, only difference is for frequency of 400 Hz when relative amplitude error for current shunt is larger. Obviously, relative amplitude error of voltage for the resistive divider is in the same order over whole frequency range which means that calculation of amplitude with interpolated DFT algorithm does not depend on these analyzed signal frequencies.

Acknowledgement

This paper is fully supported by Croatian Science Foundation under the project Metrological infrastructure for smart grid IP-2014-09-8826.

References

[1] J. Konjevod, M. Dadić, R. Malarić, I. Kunšt, “AC-DC transfer difference measurement of AC shunts”, SMAGRIMET Conference, 2018.

[2] J. Konjevod, H. Hegeduš, R. Malarić, I. Kunšt, “Switch based on relays with low operation and release time for AC-DC transfer difference measurements”, SMAGRIMET Conference, 2018.

[3] B. Voljc, M. Lindic, B. Pinter, M. Kokalj, Z. Svetik, R. Lapuh, »Evaluation of a 100 A Current Shunt for the Direct Measurement of AC Current«, IEEE Transactions on Instrumentation and Measurement, pp. 1675 – 1680, 2013.

[4] B. Voljc, M. Lindic, and R. Lapuh, »Direct Measurement of AC Current by Measuring the Voltage Drop on the Coaxial Current Shunt«, IEEE Transactions on Instrumentation and Measurement, pp. 863 – 867, 2009.

[5] M. Klonz, H. Laiz, T. Spiegel, P. Bittel, »AC-DC Current Transfer Step-up Calibration and Uncertainty Calculation«, IEEE Transactions on Instrumentation and Measurement, pp.1027-1034, 2002.

[6] M. Flueli and W. Fasel, A Fast Switching System for AC-DC Transfer Measurements, METAS, Switzerland, CONFERENCE ON PRECISION ELECTROMAGNETIC MEASUREMENTS, Washington, USA, 1998.

Journal of Energy

VOLUME 67 | 2018

journal homepage: http://journalofenergy.com/

Igor Štambuk
Center for Defense and Strategic Studies
Croatian Defense Academy "Dr. Franjo Tuđman",
Zagreb, Croatia, istambuk.edu@gmail.com

Precison Automated Measuring System for Accurate Comparison of Resistance Standards and Shunts

Summary

In this paper we will present a development of Measurement system for accurate comparison of low resistance standards and AC shunts ranging from 0.1 mΩ to 10 Ω as well as system testing and use. The system consists of a specially built current source, range selector, current reversal module and low cost analog to digital converter. The entire measurement procedure is automated and controlled by LabVIEW program. Subsequent testing has shown that the realized precision resistance measurement system has achieved precision comparable to more expensive commercial devices. The system or system elements can be used both in smart grid applications and in military laboratories for testing new technologies.

Key words: digital multimeters, measurement method, resistant standard, virtual instrumentation

Introduction

Precise impedance measurement is a key factor in many areas of science, and so far different measurement systems have been proposed: combination of commercial equipment and specific electronic circuits [1,2] and combinations of scientific commercial instruments [3,4,5] or specific systems [6,7]. However, the main difficulty in measuring mostly impedance comes when high precision is required. In this case, the width of the range is always problematic i.e., it is difficult to design a device that can meet different purposes in a wide range of resistances. There are works that have provided quality solutions for areas of 100 kΩ to 100 MΩ [8,9] and 10 kΩ to 1 TΩ [10]. For areas ranging from 0.1 mΩ to 10 Ω [11], Measurement System for accurate comparison of low resistance standards was recently developed. System is carefully designed and all electronic components used in the measuring circuit have been carefully evaluated in various situations, especially when the instruments must work properly for different metering, temperature ranges and humidity.

Labview Application for Controlling the Measurement Process

The program for controlling the measurement of small resistance of the IGMMMO is made on the LabVIEW 10.0 software platform. LabVIEW (Laboratory Virtual Instrument Engineering Workbench) is one of the most well-known development software applications from National Instruments Corporation. [12]

The IGMMMO program that communicates with the IGUS controller was implemented with the VI module »Out Port.vi« via the parallel PC interface. In normal use, the parallel port (parallel port) is most commonly used for writing to a printer or some other device connected to a computer. It sends data in a format of 8-bit or one byte in parallel at a specific time.

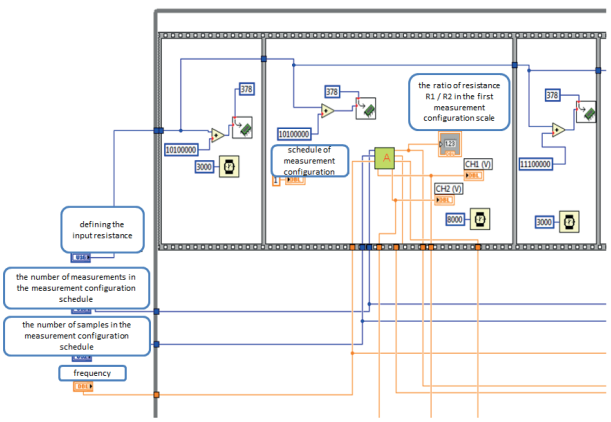

Figure 1. Labview programming time sequences

Igor Štambuk, Precison Automated Measuring System for Accurate Comparison of Resistance Standards and Shunts, vol. 67 (2018), Special Issue, p. 19–22

Current level for the measuring circuit

The current circuit power can be controlled automatically via the IGUS controller. With the IGMMMO measurement program, we can turn on and off the current to the resistances in the IGUS Module Control Module circuit by entering the corresponding four-digit combination into the main program. For example, for the inclusion of current to resistance of 1.5 Ω, the combination 1110 is written in a data combination that is addressed to the Module for Measurement Areas via the ¨Out port module. [12]

Measurement System Igmmmo

The IGMMMO method [11,13] is a specialized measurement method for measuring low resistance ratios. The method is fully automated and the resistance range that can be measured with a standard deviation of less than $1 \cdot 10^{-5}$ is from 1 mΩ to 10 Ω of rated resistance.

In order to measure the correctness, it is important to carry out the documented procedure. This procedure was followed by a series of successive measurements and tests with a new measurement system for the measurement of low resistance IGMMMO.

Figure 2. shows the basic structure of the IGMMMO measurement system.

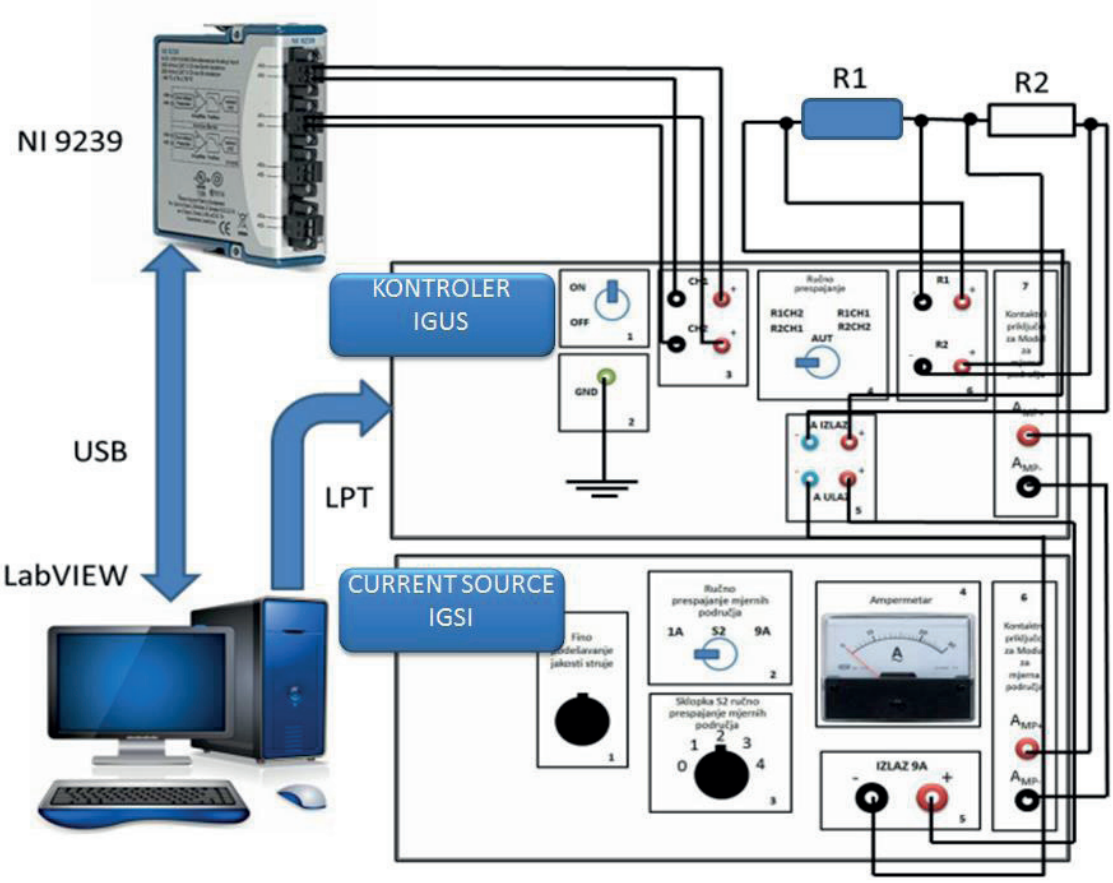

Figure 2. Measuring system IGMMMO

The system is designed to measure low resistance ratio, including the measurement resistance R1 and the known reference resistance R2. Most commonly, a known resistor is the resistance standard. The resistance of an unknown four-terminal resistor R1 is determined by measurement with the digital 24-bit A/D DAQ. It is desirable to have a standard resistor as a reference standard with four terminals, approximately the same nominal value as the resistor to be measured. The resistors are usually immersed in oil bath [14], in which the oil is stirred at a working temperature of 23 ° C, monitored by mercury glass thermometer. If we calibrate resistors that are not immersed in an oil bath to maintain the same temperature level it is desirable that the temperature in the laboratory does not vary and is maintained at 23°C. The connections of each resistor (R+, R-) are connected, via the DAQ Module for changing position of DAQ measuring channels. The measurement current is derived from a personally constructed IGSI power source and is automatically regulated through the measuring range modules. It has been determined that the measurement current is large enough for the accurate voltage drops reading at low resistances of 1 mΩ and on the other hand, it will be small enough to not cause self-heating of the resistor. The current source of IGSI is capable of producing electricity up to 9 A.

The measurement system is coupled according to Figure 2. If we measure the temperature of the resistors and in the measuring environment then we will add another DAQ measuring device with the adaptive circuit [11] and set NTC thermistor sensors to the corresponding DAQ channel. On measuring cables, i.e. cables leading to the DAQ measuring device (in our case NI 9239) it is desirable to shield and twist cable cables in order to minimize electromagnetic interference as well as external noise of the 50 Hz network.

Igus Kontroler

the most important part of the IGMMMO measuring system [12,] is the device for automated measurement control and is called the IGUS (IG controller). The device has three main purposes. Its first purpose is to regulate the power of the current through the measuring module, the second is to change the direction of the current in the measuring circuit, and the third is to change channel position of the DAQ measuring device.

The IGUS controller consists of the following modules that are separated by functional areas:

- Power Supply Module
- Measuring range module
- Module for changing direction of current
- Module for changing position of DAQ measuring channels

All these modules are built into a specially designed casing with fan cooling system and specially designed connectors for connecting with other elements of the IGMMMO measuring system.

Module for changing direction of current Module for changing position of DAQ measuring channels

Module for changing the direction of current [12,15] has the function of changing direction of current passing through measuring and reference resistor. The module is shown in Figure 3.

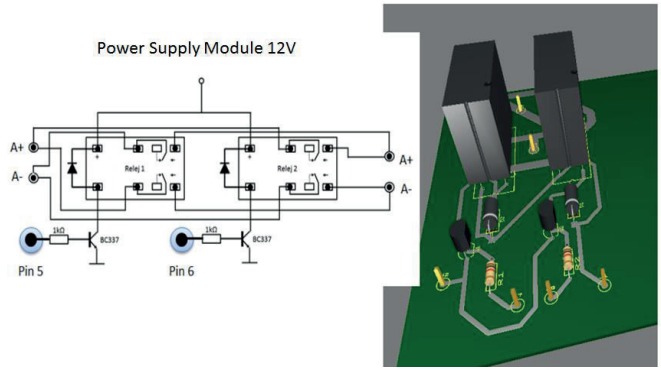

Figure 3. Current direction change module in 3D projection.

The IGUS controller is designed to affect the measurement accuracy as little as possible. The picture also shows 3D projection created using the National Instruments Ultiboard software. The IGMMMO current-changing module can be controlled via the LPT port with IGMMMO LabVIEW program. The two pins (4 and 5) control the duration of the positive and negative half-wave current as well as the duration of the non-current period.

Table I. Combinations of bits used to control the current commutation module

combination of pins		current direction
pin 4	pin 5	
0	1	positive current direction
1	0	negative current direction

Measuring the Temperature Oscilations of the Measuring Range Modul

In order to determine the temperature characteristics of the IGUS Control Unit in the measurement process in this subdivision, the results of the measurement of temperature oscillations of individual components, which are essential for proper operation of the control device, are given. Measurements were made [12] with an infrared red FLIR i7 thermo camera [16], for different loads of the measuring circuit i.e. for different current values. The results of the temperature oscillation measurement are shown for the IGUS Measuring range Module because it is subjected to the highest heating since it flows through the current I0 which is approximately the same as the measurement current, while the other modules have no significant oscillation temperature. The highest heating in the module is expected to take place on module energy resistors.

If the control bit combination (1101) is sent to the Measuring range Module, pins 1, 3 and 4 will cause a logic unit 1 to the base of the T1, T3 and T4 transistors, i.e. the voltage at which transistors will be activated and they activate the relays 1, 3 and 4. The heating of the Measuring range module in the case of a combination (1101), i.e. if the relays 1, 3 and 4 are switched on and the measuring circuit flows is 1 A, is recorded with the FLIR i7 thermo camera and the recording results are shown in Figure 4.

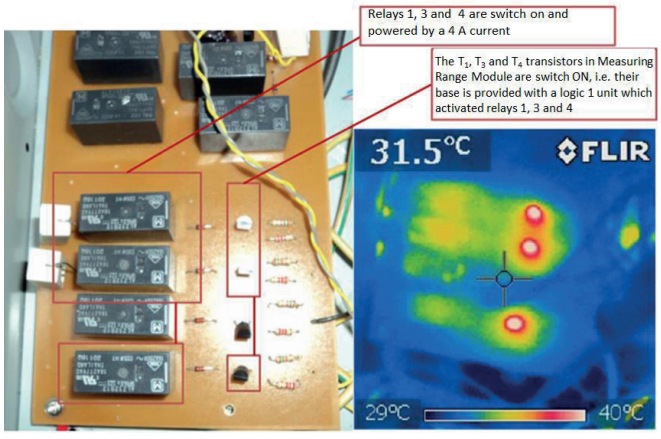

Figure 4: Thermo picture of warming up the Measuring Range Module with control panel combination (1101)

Measurement and Results Conclusion

One of the key experiments is to determine the accuracy of low-resistance measurements [12, 15, 17, 18, 19, 20, 21, and 22]. For this purpose, the IGMMMO measured the voltage drop of current shunts with nominal values of 1 mΩ and 2 mΩ. After the measurements [21], the following results were obtained - the arithmetic mean of the ratio of voltage drops on resistors was r = 0.4376, experimental standard deviation was $s(r) = 7.69 \cdot 10^{-6}$, and the standard deviation of the arithmetic mean of the ratio of resistance was $u(r) = 7.69 \cdot 10^{-7}$. Measurements at stabile temperature conditions generally have lower standard deviations. In conclusion, we see that differences in results (standard deviation), when these two measurements are compared, are small, about 0.5 μΩ/Ω. The temperature oscillations of the first measurement were within the range of 30.0°C to 30.2°C, while in the other experiment it was 23°C ± 0.1°C. The similarity between the results can be explained by the parallel rise in temperature of both measuring resistors, which have been heated proportionally, so their ratio did not oscillate as well. Table II summarizes the several methods available.

Table II. Comparison of tested methods

measured resistor	DV method (method with digital voltmeters)	DAQ method IGMMMO (a method with a DAQ measuring device)	DAQ method IGMMMO with current source IGSI
up to 1 mΩ	it is not good because of small voltage drops on measuring resistances	does not fully satisfies due to small voltage drops on measured resistors	satisfies because of the possibility of generating higher current through the measuring circuit and thus a higher voltage drop on measured resistors
1 mΩ - 1 Ω	the results are weaker than the DAQ method results	good (the results are better than the DV method) but it does not fully satisfies due to small voltage drops on measured resistors	very good (the results are better than the DV method)
1 Ω - 1 kΩ	very good	good (results are similar to those obtained with the DV method) more measurement ranges are used	very good (the results are similar to the DV method)

Based on the measurements shown in doctoral thesis[12], the measurement methods presented can be characterized by the nominal values of the resistors we measure. Comparison of measurement methods with digital voltmeters (DV method) of empirical methods with DAQ measuring devices (DAQ method) with and without connected current IGSI current strength up to 9 A, was conducted. From this comparison, it is visible that the IGMMMO DAQ method with the IGSI current source has very good results for almost all the ranges of the measured resistance shown in Table 2, while for a resistance range of 1 mΩ - 1 Ω, the results are even better than the DV method with digital voltmeters, enabling wider application of DAQ measuring devices as a replacement for expensive high-accuracy voltmeters.

Conclusion

The measurements were periodically repeated, usually one time per month, to estimate the time stability of the measuring system when measuring the resistance standards. During the test period, and according to the obtained results, it can be seen that there is very little deviation in measurement results at all-time intervals, although the results show time-nonlinear behavior, which suggests that the IGMMMO measurement system has a satisfactory time stability.

Based on the obtained results, the results of the standard deviation, and the comparison of the obtained results with the previously determined resistance values and resistance standards, we see that the IGMMMO system fully satisfies its primary task of measuring ratio of low voltage resistances of rated values in the range of 1 mΩ - 1 Ω, with a standard deviation of lower than 8 μΩ / Ω.

References

1. Putta, S.; Vaidyanathan, V.; Chung, J.; Development and testing of a nodal resistance measurement (NRM) system for composite structures, Measurement 2008, 41, 763–773. [Google Scholar] [CrossRef]
2. Silvia Casans, Alfredo Rosado-Muñoz and Taras Iakymchuk; ¨Novel Resistance Measurement Method: Analysis of Accuracy and Thermal Dependence with Applications in Fiber Materials¨
3. Kandala, C.; Nelson, S.; RF Impedance method for estimating moisture content in small samples of In-Shell peanuts. IEEE Trans. Instrum. Meas. 2007, 56, 938–943. [Google Scholar] [CrossRef]
4. Isaksson, T.; Thelandersson, S. Experimental investigation on the effect of detail design on wood moisture content in outdoor above ground applications. Build. Environ. 2013, 59, 239–249. [Google Scholar] [CrossRef]
5. Brischke, C.; Lampen, S.C. Resistance based moisture content measurements on native, modified and preservative treated wood. Eur. J. Wood Wood Prod. 2014, 72, 289–292. [Google Scholar] [CrossRef]
6. Fan, D.; Xue, J. The design of intelligent automatic test system for wood moisture content test. In Proceedings of the 2010 International Conference on Computer Design and Applications (ICCDA), Qinhuangdao, China, 25–27 June 2010; Volume 3, pp. 314–316.
7. Zhang, J.; Wang, P. Online monitoring and detecting of wood drying kilns' parameters based on embedded system. In Proceedings of the 2013 25th Chinese Control and Decision Conference (CCDC), Guiyang, China, 25–27 May 2013; pp. 4189–4193.
8. Tadros, N.N.; Ali, R.S.M. Automated accurate high value resistances measurement in the range from 100 kΩ to 100 MΩ at NIS. Measurement 2012, 45, 988–992. [Google Scholar] [CrossRef]
9. Tadros, N.N.; Ali, R.S.M. Improved system for the automatic calibration of standard resistors in the meg-ohm range. Measurement 2013, 46, 2077–2081. [Google Scholar] [CrossRef]
10. Galliana, F.; Capra, P.P.; Gasparotto, E. Metrological management of the high DC resistance scale at INRIM. Measurement 2009, 42, 314–321. [Google Scholar] [CrossRef]
11. Štambuk,I., Malaric R.; Measurement system for precise comparison of low ohmic resistance standards. Measurement. 66 (2013) ; 161-167
12. Štambuk. I.; Mjerni sustav za preciznu usporedbu etalona otpora malih nazivnih vrijednosti, PhD, FER, Zagreb, 2014.
13. I. Štambuk, R. Malaric´ , Development of 9 A current source for precise resistance measurement method, Rev. Sci. Instrum. 83 (2012).
14. R. Malarić, Maintenance of the Group Resistance Standards of the Primary Electromagnetic Laboratory, PhD, FER, Zagreb, 2001.
15. Štambuk I.; Automated low resistance measurement system suitable for DC characterization of AC shunts // Proceedings of First International Colloquium on Smart Grid Metrology 2018 (SMAGRIMET 2018) / Ivšić, Branimir ; Jurčević, Marko (ur.).
16. Technical Specifications, FLIR i7 Thermal Imaging Camera 120 120 Resolution <http://www.amazon.com/FLIR-i7-Thermal-Imaging-Resolution/dp/B003V4BE20> (02.lipnja.14).
17. Braudaway, D., »Precision Resistors: A review of the tehniques of measurement, Advantages, Disadvantages and Practical Approach«, IEEE Trans. Instrum. Meas. Vol.48, No. 5, pp. 884-888¨, October 1999.
18. Guildline Instruments Limited, Advances in High Current and Resistance Measurements, 2011 <http://www.guildline.com/Datasheet/Guildline6625ADatasheet.pdf>.
19. H. Hegeduš, R. Malaric´, P. Mostarac, I. Štambuk, Measurement of resistance ratios with digital voltmeter and DAQ Card – A comparison, CPEM Digest/Yang Sup Song (ur.). – Daejeon: IEEE, 2010, pp. 645–646.
20. Gert Rietveld, Jan van der Beek, and Ernest Houtzager, DC characterization of AC current shunts for wideband power applications, Duch metrology Institute, http://projects.npl.co.uk/power_energy/docs/5%20DC%20characterization%20of%20AC%20current%20shunts.pdf
21. David Deaver, Neil Faulkner, Characterization of the Power Coefficient of AC and DC Current Shunts
22. G. Rietveld, Ernest Houtzager, DC characterisation of ac current shunts for wideband power applications
23. EA-4/02, Evaluation of the Uncertainty of Measurement in Calibration, September 2013.
24. Hewlett-Packard, »Hewlett-Packard 3458A Multimeter Calibration Manual«.
25. Kessler-electronic, »Relais F4052-12«, dostupno na: http://www.kessler-electronic.de/Elektromechanik/Relais/elektromechanische_Relais/Finder/Serie_4052/F4052-12_i1362_31582_0.htm, (10. siječnja 2014.)
26. National instruments, »User guide and specifications: NI USB-9229/9239«, dostupno na: www.ni.com/Pdf/Manuals/372409a.pdf, (17. kolovoza 2010.)

ENERGIJA